Astronomical and Astrophysical Transactions (*AApTr*), 2021, Vol. 32, Issue 3, pp. 177–206,
ISSN 1055-6796, Photocopying permitted by license only, ©Cambridge Scientific Publishers

Orbits of 47 dwarf satellite galaxies of the Milky Way in three models of the gravitational potential with different masses

A.T. Bajkova*, V.V. Bobylev

Central (Pulkovo) Astronomical Observatory, Russian Academy of Sciences, Pulkovskoye Chaussee 65/1, St.-Petersburg, 196140 Russia

Received 1 August, 2021

The analysis of the orbits of 47 dwarf satellite galaxies of the Milky Way, built using three models of the galactic gravitational potential with different masses, is presented. The models of the galactic potential were chosen based on the analysis of a large number of the Galaxy mass estimates known from the literature. The astrometric data needed for calculation of the initial positions and velocities (6D phase space) of the dwarf galaxies are also taken from the literature, where the average proper motions were determined on the basis of the data from the Gaia DR2 Catalog. We present the orbits and their properties of all 47 dwarf galaxies obtained by integration for 13.5 Gyr backward in all three models of the galactic potential and give a comparison of the orbital parameters. For each model of the galactic potential we have identified dwarf galaxies that are not connected gravitationally with the Milky Way.

Keywords: Dwarf satellite galaxies: Galaxy (Milky Way)

1 Introduction

Our Galaxy is surrounded by a cloud of dwarf satellite galaxies (McConnachie, 2012). More than 60 such satellites are currently known in the region with a radius of about 300 kpc from the Sun (Drlica-Wagner et al., 2020). According to the analysis of the distribution of matter density in the halo and the luminosity function, the expected number of satellite galaxies should be approximately twice as large (Newton et al., 2018; Nadler et al., 2020). It is likely that the application of more sensitive technology will soon increase the number of faint dwarf satellite galaxies.

The interest in dwarf satellite galaxies of the Milky Way is associated both with their spatial distribution and with their movement. According to modern data on the satellite galaxy population, Deason et al. (2020) estimated the radius of the Milky Way halo as 292 ± 61 kpc. To determine such a "margin" of the Galaxy, these authors

*Email: bajkova@gaoran.ru

looked for a point of density or line-of-sight velocity fall both in the model distribution of dark matter or stars and in the observed distribution of dwarf satellite galaxies of the Milky Way. In the works of Pawlowski & Kroupa (2013a,b), attempts were made to detect coherent structures in the distribution and motion of dwarf galaxies of the Local Group. Of interest is the study of the evolution of the entire cloud of Milky Way satellite galaxies, the presence of plumes in the Galaxy and the search for surviving remains from the destruction of dwarf galaxies (Helmi, 2020), the analysis of the evolutionary relationship with globular clusters of the Galaxy (Massari et al., 2019).

The velocities of satellite galaxies and globular clusters, albeit indirectly (through the dispersion of velocities in the Jeans equation), were used to construct the rotation curve of the Galaxy over a very wide range of distances from the galactic center 0-200 kpc (Bhattacharjee et al., 2014). Such a rotation curve ultimately served as the basis for refining the model of the gravitational potential of the Galaxy, estimating the mass of the Galaxy (Bajkova & Bobylev, 2016; Sofue, 2017; Bobylev et al., 2017), refining the nature of the distribution of invisible matter (Pato & Iocco, 2015).

A reliable study of the kinematics of satellite galaxies requires knowledge of a number of parameters with high accuracy. The distances from variable stars with errors from 5% to 10% and line-of-sight velocities, whose errors are independent of distance, are relatively well estimated. The "weak link" here is the proper motions, since when moving from the measured velocity components in angular units (mas yr^{-1}) to linear (km s^{-1}), multiplication by distance occurs. Therefore we need to know, with minimal errors, the angular movements of dwarf galaxies-satellites of the Milky Way.

For a number of dwarf galaxies, the absolute proper motions were measured using the Hubble Space Telescope (HST) (Pryor et al., 2010, 2015; Kallivayalil et al., 2013). Random errors in determining these proper motions depend on various factors, in particular, from the difference of eras. For example, according to observations on the HST with an epoch difference of 7 years, the proper motions of the Magellanic clouds (LMC and SMC) were measured relative to quasars with errors of about 0.05 mas yr^{-1} (Kallivayalil et al., 2013). For 11 galaxies such measurements are collected in the work of Pavlovsky & Kroupa (2013a). A study of the dynamics of the Local Group using this data was performed, for example, by Pawlowski & Kroupa (2013b); van der Marel (2015); Bajkova & Bobylev (2017b).

The appearance of the Gaia DR2 Catalog (Brown et al., 2018; Lindegren et al., 2018) led to a significant increase in the number of dwarf galaxies with calculated high-precision absolute proper motions (Massari & Helmi, 2018; Fritz et al., 2018, 2019; Simon, 2018; Pace & Li, 2019). In the Gaia DR2 Catalog, the average parameter errors depend on the magnitude. For example, the average errors of proper motions range from 0.05 mas yr^{-1} for bright ($G < 15^m$) to 1.2 mas yr^{-1} for faint ($G > 20^m$) stars.

The closest to us in purpose is the work of Fritz et al. (2018) performed on the basis of the data from the Gaia DR2 Catalog and devoted to study of the orbits of 39 dwarf galaxies, calculated in two potentials with halo of low ($0.8 \times 10^{12} M_\odot$) and high mass ($1.6 \times 10^{12} M_\odot$). Our work is aimed at creating, according to literature, a more complete list of satellite galaxies with data necessary for calculating spatial velocities, and at analysis of their three-dimensional dynamics using models of the galactic potential, updated recently using modern data on the rotation curve of the Galaxy. Our list includes 47 dwarfs. The choice of the galactic gravitational potential

models for construction of the orbits is based on the estimates of the mass of the Galaxy obtained by various authors using various objects and methods of analysis. As a result, it was shown that all known estimates lie in the mass range determined by three potential models with masses $M_{G_{(R\leq 200\ kpc)}} = 0.75\times10^{12}M_{\odot}, 1.45\times10^{12}M_{\odot}$, and $1.90\times10^{12}M_{\odot}$. We integrate orbits of the dwarfs using all these three models of the galactic potential and give comparison of the orbit properties.

The work is structured as follows. Section 2 is devoted to the analysis of the galactic mass estimates from the literature and to the choice of the galactic potential models for further dynamic analysis of the dwarf galaxies. Section 3 describes the potential models and equations of motions for orbit integration. Section 4 describes data. In Section 5 we give the results obtained and their analysis. In Conclusions we summarize main results.

2 Estimates of the mass of the Galaxy from the literature

So, to select the most probable models of the galactic potential in order to integrate the orbits of dwarf satellite galaxies, we collected the Galaxy mass estimates from various literary sources obtained by independent methods, and plotted them on one graph (Fig. 1).

Most of the presented mass estimates are based on the construction of the rotation curve of the Galaxy from one or another data. To construct the rotation curve of the Galaxy, giant stars that are visible at large distances are often used. Other important objects for solving this problem are Cepheids, stars of the RR Lyra type, globular clusters, or dwarf satellite galaxies of the Milky Way.

In the paper by Dehnen & Binney (1998), a Galaxy rotation curve was constructed up to a distance of $R = 100$ kpc using a variety of data. In particular, data on the velocities of the H II, Cepheids, and dwarf galaxies were used. The data on proper motions were taken from the HIPPARCOS Catalog (1997). A three-component axisymmetric model of the gravitational potential was used to determine the law of density distribution in the Galaxy. The same method was later applied by McMillan (2011).

In the work of Kafle et al. (2012), the line-of-sight velocities of more than 4500 blue branch giants with distances R up to 60 kpc were taken. These are stars from the SDSS Catalog (Aihara et al., 2011) with line-of-sight velocities from the SEGUE Catalog (Yanny et al., 2009). To fit the rotation curve, they used a three-component axisymmetric model of the galactic potential, including the bulge, disk, and halo. The mass of the Galaxy was estimated on the basis of the Jeans equation by the radial velocity dispersion profile, the anisotropy profile, and the density distribution law. Figure 1 gives two estimates by these authors – for $R = 25$ kpc and $R = 249$ kpc.

According to the data on blue giants of the horizontal branch from the SDSS Catalog, Deason et al. (2012a) obtained an estimate $M_{G_{(R\leq 50\ kpc)}} = (0.42\pm0.04)\times 10^{12}M_{\odot}$. In another work by these authors (Deason et al., 2012b), $M_{G_{(R\leq 150\ kpc)}} = (0.5-1.0)\times10^{12}M_{\odot}$ was found from farther blue giants of the horizontal branch.

Xue et al. (2008) analyzed the line-of-sight velocities of the blue giants, which were located at distances $R < 60$ kpc. A three-component model of the galactic potential

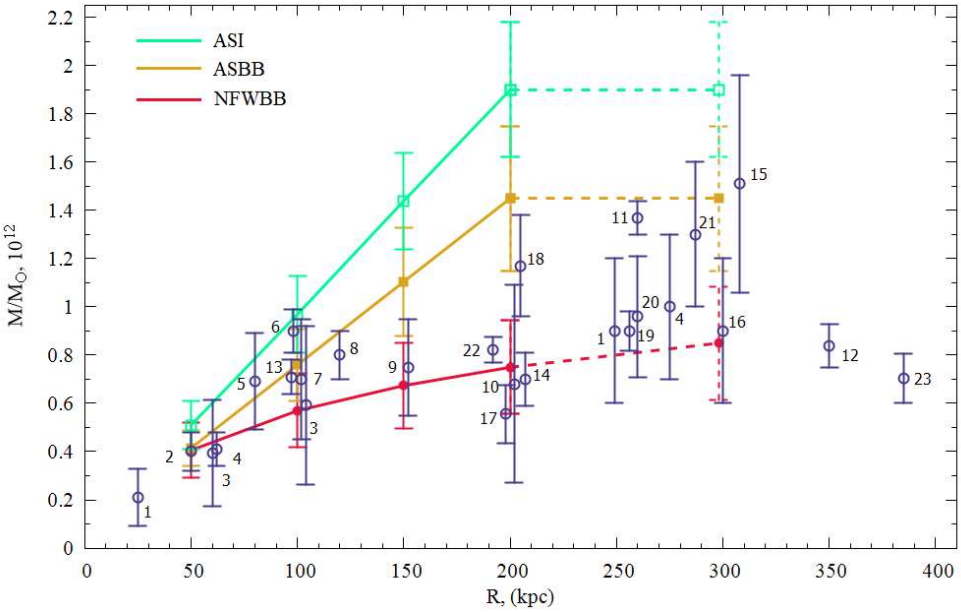


Figure 1 Estimates of the mass of the Galaxy obtained by various authors: 1 – Kafle et al. (2012), 2 – Deason et al. (2012a), 3 – Bhattacharjee et al. (2013), 4 – Xue et al. (2008), 5 – Gnedin et al. (2010), 6 – McMillan (2011), 7 – Dehnen & Binney (1998), 8 – Battaglia et al. (2005), 9 – Deason et al. (2012b), 10 – Bhattacharjee et al. (2014), 11 – Eadie et al. (2015), 12 – Karachentsev et al. (2009), 13 – Fardal et al. (2019), 14 – Eadie et al. (2019), 15 – Fritz et al. (2020), 16 – Watkins et al. (2010), 17 – Gibbons et al. (2014), 18 – Callingham et al. (2019), 19 – Huang et al. (2016), 20 – Patel et al. (2018), 21 – Posti & Helmi (2019), 22 – Ablimit et al. (2020), 23 – Sofue (2012). A description of three potential models (NFWBB, ASBB, ASI) is given in the text.

was constructed in which the halo of dark matter is presented in the Navarro-Frank-White form (Navarro et al., 1997). These authors estimated the virial mass of the Galaxy as $M_{G_{(R\leq R_{vir})}} = (1.0^{+0.3}_{-0.2}) \times 10^{12} M_\odot$, where the value of the virial radius was $R_{vir} = 275^{+23}_{-20}$ kpc. Two estimates of these authors are given in Fig. 1 – for $R = 55$ kpc and $R = 275$ kpc.

Huang et al. (2016) used about 16000 giants from redshifts LEGUE Catalog (Deng et al., 2012) and about 5700 giants of the spectral class K from the SDSS Catalog. These authors estimated the virial mass of the Galaxy as $M_{G_{(R\leq R_{vir})}} = (0.90^{+0.07}_{-0.08}) \times 10^{12} M_\odot$, where the value of the virial radius is $R_{vir} = 255.7^{+7.7}_{-7.7}$ kpc.

Fardal et al. (2019) used a sample of stars of the RR Lyra type from the Pan-STARRS1 Catalog (Hernitschek et al., 2017) to trace the Sagittarius Stream (Sgr Stream). As a result, these authors found $M_{G_{(R\leq 60\ kpc)}} = (0.41 \pm 0.04) \times 10^{12} M_\odot$ and $M_{G_{(R\leq 100\ kpc)}} = (0.71 \pm 0.07) \times 10^{12} M_\odot$.

Gibbons et al. (2014) from the analysis of Sagittarius Stream, received an estimate $M_{G_{(R\leq 100\ kpc)}} = (0.41 \pm 0.04) \times 10^{12} M_\odot$, which was extrapolated to 200 kpc, and found $M_{G_{(R\leq 200\ kpc)}} = (0.56 \pm 0.12) \times 10^{12} M_\odot$.

Gnedin et al. (2010) considered a galactic rotation curve up to distances $R = 80$ kpc constructed using the line-of-sight velocities of distant halo stars.

Battaglia et al. (2005) used line-of-sight velocities of 240 halo stars.

In the works of Bhattacharjee et al. (2013), line-of-sight velocities of globular clusters and dwarf galaxies were used to construct a galactic rotation curve at large distances. Bhattacharjee et al. (2014) found an estimate $M_{G_{(R\leq 200\ kpc)}} = (0.68 \pm 0.41) \times 10^{12} M_{\odot}$.

Eadie et al. (2015) estimated the mass of the Galaxy as $M_{G_{(R\leq 260\ kpc)}} = (1.37 \pm 0.07) \times 10^{12} M_{\odot}$ according to data on globular clusters and dwarf galaxies located up to $R = 260$ kpc.

Eadie & Jurić (2019) used the latest data on globular clusters.

Fritz and coauthors (2020) obtained a virial estimate of the mass of the Galaxy $M_{G_{(R\leq R_{vir})}} = (1.51^{+0.45}_{-0.40}) \times 10^{12} M_{\odot}$ from data on dwarf galaxies, where $R_{vir} = 308$ kpc. Their work provides a fairly complete overview of the results of determining the mass of the Galaxy by various authors.

Watkins et al. (2010) used data on halo stars, globular clusters and dwarf galaxies and found $M_{G_{(R\leq 300\ kpc)}} = (0.9 \pm 0.3) \times 10^{12} M_{\odot}$.

Callingham et al. (2019) obtained $M_{G_{(R\leq 200\ kpc)}} = (1.17^{+0.21}_{-0.15}) \times 10^{12} M_{\odot}$ from data on dwarf galaxies satellites of the Milky Way.

Patel et al. (2018) found $M_{G_{(R\leq 260\ kpc)}} = (0.96^{+0.29}_{-0.28}) \times 10^{12} M_{\odot}$ from data on dwarf galaxies satellites of the Milky Way.

Posti & Helmi (2019) obtained a virial estimate of the mass of the Galaxy as $M_{G_{(R\leq R_{vir})}} = (1.3 \pm 0.3) \times 10^{12} M_{\odot}$, where $R_{vir} = 287^{+22}_{-25}$ kpc.

Ablimit et al. (2020) used about 3500 classical Cepheids with data from the OGLE catalogs (Optical Gravitational Lensing Experiment) (Udalski et al., 1997), ASAS (All Sky Automated Survey) (Pojmanski, 2002) and Gaia DR2 (Prusti et al., 2016; Brown et al., 2018) to construct the rotation curve of the Galaxy. These authors obtained a virial estimate of the mass of the Galaxy $M_{G_{(R\leq 192\ kpc)}} = (0.822 \pm 0.052) \times 10^{12} M_{\odot}$.

Based on a three-component model of the galactic potential in which the halo of dark matter is presented in the Navarro–Frenk–White form (Navarro et al., 1997), Sofue (2012) obtained a virial estimate of the mass of the Galaxy $M_{G_{(R\leq 385\ kpc)}} = (0.70 \pm 0.10) \times 10^{12} M_{\odot}$, where half of the distance to the Andromeda nebula was chosen as an estimate of the virial radius.

Karachentsev et al. (2009) estimated the total mass of the Local Group $(19 \pm 0.2) \times 10^{12} M_{\odot}$ and the ratio of the Milky Way and M31 masses as 4:5. For this assessment, the braking effect of the local Hubble stream and data on the distances and line-of-sight velocities of galaxies in the vicinity of the Local Group were used. The total mass of the Galaxy obtained by this independent method is $M_{G_{(R\leq 350\ kpc)}} = (0.84 \pm 0.09) \times 10^{12} M_{\odot}$. Note that a similar independent analysis of galactic mass estimates is given in a recent paper by Wang et al. (2020).

Figure 1 shows three functions of the mass of the Galaxy versus the distance R, corresponding to three models of the Galactic potential, chosen by us, which cover, taking into account the error bars, almost the entire range of given estimates of the Galaxy mass. The lower curve corresponds to the model of the potential with a dark halo in the form of Navarro–Frenk–White (Navarro et al., 1997), modified by Bajkova & Bobylev (2016). The mass of the Galaxy according to this model is $M_{G_{(R\leq 200kpc)}} = 0.75 \pm 0.19 \times 10^{12} M_{\odot}$. For brevity, we designate this model as NFWBB.

The middle curve corresponds to the Allen & Santillán (1991) model of the potential, also modified in Bajkova & Bobylev (2016). The mass of the Galaxy in this model, designated as ASBB, is $M_{G_{(R\leq 200kpc)}} = 1.45 \pm 0.30 \times 10^{12} M_\odot$. And finally, the third model, with the largest mass of the Galaxy, equal to $M_{G_{(R\leq 200\ kpc)}} = 1.9^{+2.4}_{-0.8} \times 10^{12} M_\odot$, corresponds to the upper curve. The third model is the Allen & Santillán (1991) model modified by Irrgang et al. (2013). We designate it as ASI model. A more detailed description of these models is given in Section 3.1.

3 Method

3.1 The models of the galactic gravitational potential

In all of the models here, the axially symmetric gravitational potential of the Galaxy is represented as the sum of three components – the central, spherical bulge $\Phi_b(r(R,Z))$, the disk $\Phi_d(r(R,Z))$, and the massive, spherical dark-matter halo $\Phi_h(r(R,Z))$:

$$\Phi(R,Z) = \Phi_b(r(R,Z)) + \Phi_d(r(R,Z)) + \Phi_h(r(R,Z)). \tag{1}$$

Here, we use a cylindrical coordinate system (R, ψ, Z) with its origin at the galactic center. In Cartesian coordinates (X, Y, Z) with their origin at the galactic center, the distance to a star (the spherical radius) is $r^2 = X^2 + Y^2 + Z^2 = R^2 + Z^2$. The gravitational potential is expressed in units of 100 km^2 s^{-2}, distances in kpc, masses in units of the mass of the Galaxy, $M_{gal} = 2.325 \times 10^7 M_\odot$, and the gravitational constant is taken to be $G = 1$.

We express the potentials of the bulge, $\Phi_b(r(R,Z))$, and disk, $\Phi_d(r(R,Z))$, in the form suggested by Miyamoto & Nagai (1975):

$$\Phi_b(r) = -\frac{M_b}{(r^2 + b_b^2)^{1/2}}, \tag{2}$$

$$\Phi_d(R,Z) = -\frac{M_d}{\left[R^2 + \left(a_d + \sqrt{Z^2 + b_d^2}\right)^2\right]^{1/2}}, \tag{3}$$

where M_b, M_d are the masses of these components, and b_b, a_d, b_d are the scale parameters of the components in kpc.

For description of the halo component, we used (i) the expression in Navarro–Frenk–White (NFW) form presented in Navarro et al. (1997):

$$\Phi_h(r) = -\frac{M_h}{r} \ln\left(1 + \frac{r}{a_h}\right), \tag{4}$$

(where M_h is the mass and a_h is the scale length), and (ii) the expression for Allen & Santillán (1991) model (AS) derived by Irrgang et al. (2013) from the expression

for the halo mass (Allen & Martos, 1986):

$$\Phi_h(r) = \begin{cases} \dfrac{M_h}{a_h}\left(\dfrac{1}{(\gamma-1)}\ln\left(\dfrac{1+(r/a_h)^{\gamma-1}}{1+(\Lambda/a_h)^{\gamma-1}}\right) - \right. \\ \qquad \left. - \dfrac{(\Lambda/a_h)^{\gamma-1}}{1+(\Lambda/a_h)^{\gamma-1}}\right), \quad \text{if } r \le \Lambda \\ -\dfrac{M_h}{r}\dfrac{(\Lambda/a_h)^{\gamma}}{1+(\Lambda/a_h)^{\gamma-1}}, \qquad \text{if } r > \Lambda, \end{cases} \tag{5}$$

where M_h is the mass, a_h is the scale length, the galactocentric distance is $\Lambda = 200$ kpc, and the dimensionless coefficient $\gamma = 2.0$.

The first model (NFWBB) of the galactic potential, considered in this work, is the NFW model modified in work of Bajkova & Bobylev (2016) by fitting of the model parameters to data on HI, maser sources and galactic objects from Bhattacharjee et al. (2014) at distances R within ~ 200 kpc. In addition the constraints (Irrgang et al., 2013) on the local dynamical matter density $\rho_\odot = 0.1 M_\odot$ pc^{-3} and the force acting perpendicularly to the galactic plane $|K_{z=1.1}|/2\pi G = 77 M_\odot$ pc^{-2} were used.

The second model (ASBB) is the AS model modified also in work of Bajkova & Bobylev (2016) using the same data and the same local constraints.

Note that among six models of the galactic potential summarized in Bajkova & Bobylev (2017a) the NFWBB model ensures the best fit to the data.

The third model (ASI), considered in this work, is the AS model modified by Irrgang et al. (2013) using data on HI, CO and maser sources at distances up to 20 kpc and the same local constraints as in previous cases.

Parameters of these three models are given in Table 1, where local parameters $R_\odot$, $V_\odot$ and the total mass of the Galaxy within a sphere of radius 200 kpc are indicated as well. The mass distribution is shown in Fig. 1. Corresponding rotation curves up to $R = 200$ kpc are shown in Fig. 2.

Table 1 Parameters of the models of the galactic potential ($M_0 = 2.325 \times 10^7\, M_\odot$).

Parameter	NFWBB	ASBB	ASI
M_b [M_0]	443±27	386±10	409±63
M_d [M_0]	2798±84	3092±62	2856^{+376}_{-202}
M_h [M_0]	12474±3289	452±83	1018^{+27933}_{-603}
b_b [kpc]	0.267±0.009	0.249±0.006	0.23±0.03
a_d [kpc]	4.40±0.73	3.67±0.16	$4.22^{+0.53}_{-0.99}$
b_d [kpc]	0.308±0.005	0.305±0.003	$0.292^{+0.020}_{-0.025}$
a_h [kpc]	7.7±2.1	1.52±0.18	$2.562^{+25.963}_{-1.419}$
Λ [kpc]	–	200	200^{+0}_{-83}
γ	–	2.0	2.0
$R_\odot$ [kpc]	8.30	8.30	8.33
$V_\odot$ [km s^{-1}]	243.9	239.0	242.0
$M_{G_{(R\le 200kpc)}}$ [$10^{12} M_\odot$]	0.75±0.19	1.45±0.30	$1.90^{+2.4}_{-0.8}$

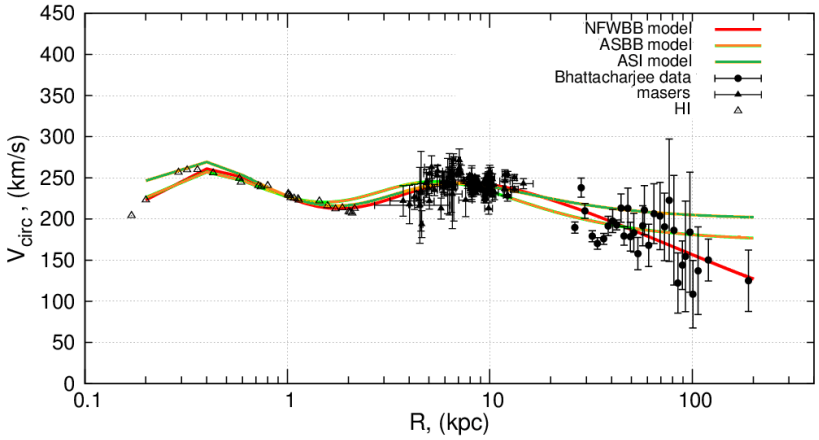


Figure 2 Rotation curves of three potential models (NFWBB, ASBB, ASI).

3.2 Integrating of the orbits and computing of their parameters

The equation of motion of a test particle in an axially symmetric gravitational potential can be obtained from the Lagrangian of the system $\pounds$ (see also Appendix A in Irrgang et al. (2013)):

$$\begin{aligned}\pounds(R, Z, \dot{R}, \dot{\psi}, \dot{Z}) = \\ 0.5(\dot{R}^2 + (R\dot{\psi})^2 + \dot{Z}^2) - \Phi(R, Z).\end{aligned} \tag{6}$$

Introducing the canonical moments

$$\begin{aligned}p_R &= \partial\pounds/\partial\dot{R} = \dot{R}, \\ p_\psi &= \partial\pounds/\partial\dot{\phi} = R^2\dot{\psi}, \\ p_Z &= \partial\pounds/\partial\dot{Z} = \dot{Z},\end{aligned} \tag{7}$$

we obtain the Lagrangian equations in the form of a system of six first-order differential equations:

$$\begin{aligned}\dot{R} &= p_R, \\ \dot{\psi} &= p_\psi/R^2, \\ \dot{Z} &= p_Z, \\ \dot{p_R} &= -\partial\Phi(R, Z)/\partial R + p_\psi^2/R^3, \\ \dot{p_\psi} &= 0, \\ \dot{p_Z} &= -\partial\Phi(R, Z)/\partial Z.\end{aligned} \tag{8}$$

We integrated Eqs. (8) using a fourth-order Runge–Kutta algorithm.

The Sun's peculiar velocity with respect to the Local Standard of Rest was taken to be $(u_\odot, v_\odot, w_\odot) = (11.1, 12.2, 7.3) \pm (0.7, 0.5, 0.4)$ km s^{-1} (Schönrich et al., 2010). Here, we use the heliocentric velocities in a moving Cartesian coordinate system with u directed towards the galactic center, v in the direction of the galactic rotation, and w perpendicular to the galactic plane and directed towards the north galactic pole.

Let the initial positions and space velocities (6D phase space) of a test particle in the heliocentric coordinate system be $(x_o, y_o, z_o, u_o, v_o, w_o)$. The initial positions

(X, Y, Z) and velocities (U, V, W) of the test particle in galactic Cartesian coordinates are then given by the formulas:

$$\begin{aligned} &X = R_\odot - x_o, Y = y_o, Z = z_o + h_\odot, \\ &R = \sqrt{X^2 + Y^2}, \\ &U = u_o + u_\odot, \\ &V = v_o + v_\odot + V_\odot, \\ &W = w_o + w_\odot, \end{aligned} \tag{9}$$

where $R_\odot$ and $V_\odot$ are the galactocentric distance and the linear velocity of the Local Standard of Rest around the galactic center, $h_\odot = 16$ pc (Bobylev & Bajkova, 2016) is the height of the Sun above the galactic plane, Π and Θ are radial and tangential velocities respectively.

Below in Table 4 the following orbital parameters of dwarf satellite galaxies are given:
(1) initial distance of the dwarf galaxy from the galactic center d_{GC}:

$$d_{GC} = \sqrt{X^2 + Y^2 + Z^2}; \tag{10}$$

(2) radial velocity Π:

$$\Pi = -U\frac{X}{R} + V\frac{Y}{R}; \tag{11}$$

(3) tangential velocity Θ:

$$\Theta = U\frac{Y}{R} + V\frac{X}{R}; \tag{12}$$

(4) total 3D velocity V_{tot}:

$$V_{tot} = \sqrt{\Pi^2 + \Theta^2 + W^2}; \tag{13}$$

(5) apocentric distance (apo) of the orbit;
(6) pericentric distance (peri) of the orbit;
(7) the eccentricity (ecc) of the orbit:

$$ecc = \frac{apo - peri}{apo + peri}; \tag{14}$$

(8) the components of the angular momentum:

$$L_X = Y \times W - Z \times V; \tag{15}$$

$$L_Y = Z \times U - X \times W; \tag{16}$$

$$L_Z = X \times V - Y \times U; \tag{17}$$

(9) inclination of the orbit θ:

$$\theta = \arccos(\frac{L_Z}{L}), \tag{18}$$

where $L = \sqrt{L_X^2 + L_Y^2 + L_Z^2}$;

(10) period of the orbit T_r;
(11) total energy E:

$$E = \Phi(R, Z) + \frac{V_{tot}^2}{2}. \quad (19)$$

The uncertainties of the parameters were calculated by the Monte-Carlo simulation using 100 iterations, taking into account the uncertainties in the initial coordinates and velocities of dwarf galaxies, as well as errors in the peculiar velocity of the Sun.

4 Data

The average values of the proper motions of dwarf galaxies were calculated according to the Gaia DR2 Catalog in the works of various authors (Simon, 2018; Massari & Helmi, 2018; Kallivayalil et al., 2018; Pace & Li, 2019; Fritz et al., 2018, 2019). Fritz et al. (2018) compared their calculations with a number of the indicated works and concluded that in most cases there is good agreement of the results within the limits of errors at the level of 1 sigma. These authors noted a difference of more than 2.5 sigma for the Cra II, and Tuc III galaxies compared with the definitions of Kallivayalil et al. (2018), possibly related to the influence of background stars. They also noted a very faint Segue 2 galaxy, whose foreground stars interfere with reliable selection of members.

Our main worklist is the work of Fritz et al. (2018), from which data on 39 galaxies were taken. For the galaxy UMi I, there are average values of proper motions in both Fritz et al. (2018) and Pace et al. (2020). These values are consistent with each other within the error of their determination. To derive the average values of the proper motions of the galaxy UMi I Fritz et al. (2018) used 137 stars common with the Gaia DR2 catalog. We preferred data from the work of Pace et al. (2020), where 892 stars (with a probability of belonging to the galaxy of more than 0.95) were refined with an analysis of the line-of-sight velocities of stars and photometric data from several surveys.

For four other galaxies, ColI, HorII, PhxII and RetIII, from Fritz et al. (2019), not only new estimates of proper motions were taken, but also distance estimates, as well as line-of-sight velocities. Finally, the list was supplemented by new estimates of the proper motions of the following galaxies: LMC and SMC (Helmi et al., 2018), Boo III (Massari & Helmi, 2018) and SgrII (Longeard et al., 2020).

The worklist thus formed (see Table 2) contains measurement data and their errors on 47 dwarf galaxies. The initial position and velocity coordinates (x_o, y_o, z_o, u_o, v_o, w_o) calculated from these data and used for integrating of the orbits are given in Table 3. Uncertainties in the initial coordinates were calculated using Monte-Carlo simulation (1000 iterations) taking into account the measurement errors. The uncertainty in the dwarf galaxies heliocentric distances d was adopted as 7% from d.

Table 2 Astrometric data for dwarf galaxies.

Name	α [deg]	δ [deg]	d [kpc]	μ_α^* [mas yr^{-1}]	$\epsilon_{\mu_\alpha^*}$ [mas yr^{-1}]	μ_δ [mas yr^{-1}]	ϵ_{μ_δ} mas yr^{-1}]	V_r [km s^{-1}]	ϵ_{V_r} [km s^{-1}]
AquII	338.48	–8.67	107.90	–0.252	0.063	0.011	0.063	–71.1	2.5
BooI	210.00	14.50	66.38	–0.554	0.035	–1.111	0.035	99.0	2.1
BooII	209.50	12.85	41.17	–2.686	0.056	–0.530	0.056	–117.0	5.2
BooIII	209.28	26.78	50.00	–1.210	0.130	–0.920	0.000	197.5	3.8
CVenI	202.01	33.56	211.27	–0.159	0.035	–0.067	0.035	30.9	0.6
CVenII	194.29	34.32	160.40	–0.342	0.056	–0.473	0.056	–128.9	1.2
CarI	100.44	–49.05	102.93	0.485	0.035	0.131	0.035	229.1	0.1
CarII	114.11	–56.00	36.20	1.867	0.035	0.082	0.035	477.2	1.2
CarIII	114.63	–56.10	27.80	3.046	0.057	1.565	0.057	284.6	3.4
CBerI	186.75	23.90	41.76	0.471	0.035	–1.716	0.035	98.1	0.9
ColI	82.86	–27.97	182.00	0.250	0.240	–0.440	0.330	153.7	5.0
CraI	174.07	–9.12	144.97	–0.045	0.063	–0.165	0.063	149.3	1.2
CraII	177.31	–17.59	117.50	–0.184	0.035	–0.106	0.035	87.5	0.4
DraI	260.06	57.92	79.18	–0.012	0.035	–0.158	0.035	–291.0	0.1
DraII	238.20	64.57	20.00	1.242	0.057	0.845	0.057	–347.6	1.8
EriII	56.09	–42.47	362.90	0.159	0.053	0.372	0.053	75.6	2.4
FnxI	39.97	–33.49	138.77	0.374	0.035	–0.401	0.035	55.3	0.3
GruI	344.18	–49.84	119.75	–0.261	0.046	–0.437	0.046	–140.5	2.4
HerI	247.76	12.79	134.71	–0.297	0.035	–0.329	0.035	45.0	1.1
HorI	43.88	–53.88	79.00	0.891	0.058	–0.550	0.058	112.8	2.6
HorII	49.13	–49.98	76.00	1.520	0.250	–0.470	0.390	168.7	12.9
HyaII	185.43	–30.01	134.00	–0.416	0.061	0.134	0.061	303.1	1.4
HyiI	37.39	–78.69	27.64	3.733	0.035	–1.605	0.035	80.4	0.6
LeoI	152.12	12.31	269.07	–0.086	0.035	–0.128	0.035	282.5	0.5
LeoII	168.37	22.15	224.39	–0.025	0.035	–0.173	0.035	78.0	0.1
LeoIV	173.24	0.53	154.23	–0.590	0.059	–0.449	0.059	132.3	1.4
LeoV	172.79	2.22	173.09	–0.097	0.057	–0.628	0.057	173.3	3.1
LMC	80.89	–68.24	50.00	1.850	0.030	0.234	0.030	262.2	3.4
PheII	355.00	–53.59	80.00	0.500	0.120	–1.160	0.140	32.4	3.8
PhxI	27.78	–43.56	418.87	0.079	0.040	–0.049	0.040	–21.2	1.0
PisII	344.63	5.95	183.01	–0.108	0.061	–0.586	0.061	–226.5	2.7
RetII	53.93	–53.95	30.00	2.398	0.035	–1.319	0.035	62.8	0.5
RetIII	56.36	–59.55	92.00	–0.390	0.530	–0.320	0.630	274.2	7.5
SgrI	283.76	–29.52	26.00	–2.736	0.035	–1.357	0.035	140.0	2.0
SgrII	298.17	–21.93	67.00	–0.650	0.100	–0.880	0.120	–177.3	1.2
SclI	15.03	–32.33	84.77	0.084	0.035	–0.133	0.035	111.4	0.1
Seg1	151.76	16.07	23.02	–1.697	0.035	–3.501	0.035	208.5	0.9
Seg2	34.82	20.18	36.09	1.656	0.045	0.135	0.045	–39.2	2.5
SMC	13.16	–71.20	64.00	0.797	0.030	–1.220	0.030	145.6	0.6
SxtI	153.26	–0.39	85.74	–0.438	0.035	0.055	0.035	22ing4.2	0.1
TriII	33.32	36.18	30.00	0.588	0.051	0.554	0.051	–381.7	1.1
TucII	342.98	–57.43	57.00	0.910	0.035	–1.159	0.035	–129.1	3.5
TucIII	359.15	–58.40	25.00	–0.025	0.035	–1.661	0.035	–102.3	2.0
UMaI	158.72	51.92	97.34	–0.683	0.035	–0.720	0.035	–55.3	1.4
UMaII	132.87	63.13	34.88	1.691	0.035	–1.902	0.035	–116.5	1.9
UMiI	227.27	67.24	76.22	–0.152	0.014	0.064	0.013	–244.7	0.3
Wil1	162.34	51.05	38.28	0.199	0.053	–1.342	0.053	–12.3	2.5

Table 3 Dwarf galaxies 6D phase space coordinates.

Name	x_o [kpc]	y_o [kpc]	z_o [kpc]	u_o [km/s]	v_o [km/s]	w_o [km/s]
AquII	$38.0^{+2.6}_{-2.8}$	$53.3^{+3.7}_{-3.9}$	$-85.8^{+6.2}_{-5.9}$	$80.7^{+30.3}_{-31.7}$	$-3.3^{+27.2}_{-29.7}$	$123.2^{+19.3}_{-21.3}$
BooI	$23.0^{+1.6}_{-1.8}$	$-1.4^{+0.1}_{-0.1}$	$62.2^{+4.4}_{-4.7}$	$103.2^{+11.3}_{-11.8}$	$-385.1^{+32.0}_{-28.4}$	$58.6^{+5.2}_{-5.0}$
BooII	$14.7^{+1.0}_{-1.0}$	$-2.0^{+0.1}_{-0.1}$	$38.4^{+2.6}_{-2.7}$	$-377.2^{+26.4}_{-24.3}$	$-396.1^{+29.8}_{-29.1}$	$-1.9^{+9.1}_{-9.9}$
BooIII	$10.5^{+0.7}_{-0.8}$	$7.0^{+0.5}_{-0.5}$	$48.4^{+3.3}_{-3.5}$	$-37.7^{+23.6}_{-24.0}$	$-317.3^{+31.4}_{-30.2}$	$258.3^{+9.7}_{-9.8}$
CVenI	$11.1^{+0.8}_{-0.8}$	$35.7^{+2.4}_{-2.5}$	$207.9^{+14.2}_{-14.5}$	$-86.9^{+34.7}_{-35.4}$	$-140.2^{+34.7}_{-35.1}$	$60.1^{+6.5}_{-6.4}$
CVenII	$-7.6^{+0.6}_{-0.5}$	$18.9^{+1.3}_{-1.4}$	$159.1^{+10.8}_{-11.6}$	$-24.0^{+43.1}_{-42.9}$	$-455.1^{+54.5}_{-50.9}$	$-77.1^{+6.4}_{-6.8}$
CarI	$-22.2^{+1.6}_{-1.5}$	$-93.1^{+6.7}_{-6.4}$	$-38.0^{+2.7}_{-2.6}$	$-62.8^{+16.7}_{-16.9}$	$-296.9^{+9.8}_{-9.3}$	$143.2^{+22.1}_{-23.4}$
CarII	$-2.1^{+0.1}_{-0.1}$	$-34.7^{+2.3}_{-2.4}$	$-10.2^{+0.7}_{-0.7}$	$87.5^{+9.7}_{-10.1}$	$-547.8^{+6.4}_{-6.8}$	$151.2^{+21.2}_{-20.0}$
CarIII	$-1.5^{+0.1}_{-0.1}$	$-26.7^{+1.8}_{-1.7}$	$-7.7^{+0.5}_{-0.5}$	$-40.2^{+7.4}_{-7.2}$	$-396.8^{+9.2}_{-8.5}$	$354.4^{+28.3}_{-30.3}$
CBerI	$-2.3^{+0.2}_{-0.1}$	$-4.0^{+0.3}_{-0.3}$	$41.5^{+2.7}_{-2.9}$	$240.1^{+17.5}_{-18.4}$	$-261.9^{+18.9}_{-18.4}$	$86.5^{+1.4}_{-1.4}$
ColI	$-102.4^{+7.2}_{-7.2}$	$-122.1^{+8.6}_{-8.6}$	$-87.8^{+6.1}_{-6.2}$	$211.4^{+229.7}_{-228.0}$	$-411.7^{+182.4}_{-177.6}$	$7.5^{+179.3}_{-187.3}$
CraI	$3.5^{+0.2}_{-0.2}$	$-94.2^{+6.2}_{-6.5}$	$110.1^{+7.6}_{-7.2}$	$29.1^{+42.6}_{-41.2}$	$-183.8^{+35.2}_{-33.4}$	$38.3^{+30.0}_{-28.6}$
CraII	$16.5^{+1.2}_{-1.2}$	$-84.6^{+6.1}_{-5.9}$	$79.8^{+5.6}_{-5.8}$	$-52.4^{+19.4}_{-18.8}$	$-137.3^{+13.8}_{-14.2}$	$-6.0^{+14.2}_{-14.8}$
DraI	$5.8^{+0.4}_{-0.4}$	$64.8^{+4.2}_{-4.5}$	$45.1^{+2.9}_{-3.1}$	$36.8^{+13.6}_{-14.9}$	$-248.1^{+7.8}_{-7.8}$	$-159.1^{+11.1}_{-11.0}$
DraII	$-1.7^{+0.1}_{-0.1}$	$14.6^{+1.1}_{-1.0}$	$13.6^{+1.0}_{-0.9}$	$8.8^{+5.3}_{-5.5}$	$-158.1^{+7.9}_{-7.5}$	$-340.6^{+8.2}_{-8.5}$
EriII	$-89.2^{+6.5}_{-6.4}$	$-205.7^{+14.9}_{-14.7}$	$-285.3^{+20.7}_{-20.4}$	$-690.5^{+95.6}_{-98.6}$	$107.3^{+76.0}_{-77.0}$	$42.4^{+57.0}_{-55.1}$
FnxI	$-34.0^{+2.3}_{-2.2}$	$-45.6^{+3.1}_{-3.0}$	$-126.6^{+8.7}_{-8.2}$	$15.6^{+21.9}_{-20.9}$	$-358.9^{+33.0}_{-31.6}$	$64.3^{+11.7}_{-12.5}$
GruI	$58.0^{+4.1}_{-4.0}$	$-23.8^{+1.6}_{-1.7}$	$-102.0^{+7.0}_{-7.2}$	$95.9^{+25.2}_{-26.2}$	$-165.7^{+28.5}_{-29.6}$	$258.1^{+16.8}_{-17.3}$
HerI	$95.9^{+6.6}_{-6.4}$	$49.3^{+3.4}_{-3.3}$	$80.8^{+5.6}_{-5.4}$	$109.6^{+16.0}_{-15.5}$	$-247.0^{+25.7}_{-26.9}$	$95.5^{+18.3}_{-17.9}$
HorI	$-0.4^{+0.0}_{-0.0}$	$-45.5^{+3.1}_{-3.3}$	$-64.6^{+4.4}_{-4.7}$	$-40.4^{+22.0}_{-23.9}$	$-383.9^{+26.5}_{-29.1}$	$132.3^{+20.6}_{-18.6}$
HorII	$-7.1^{+0.5}_{-0.5}$	$-43.9^{+3.2}_{-3.1}$	$-61.6^{+4.4}_{-4.3}$	$-174.7^{+130.1}_{-118.8}$	$-537.1^{+87.0}_{-92.8}$	$195.0^{+62.7}_{-59.0}$
HyaII	$45.6^{+3.1}_{-3.1}$	$-103.5^{+7.0}_{-7.0}$	$71.8^{+4.9}_{-4.9}$	$-157.5^{+39.8}_{-42.6}$	$-320.7^{+24.8}_{-26.7}$	$203.2^{+31.9}_{-33.1}$
HyiI	$9.5^{+0.7}_{-0.7}$	$-19.8^{+1.4}_{-1.4}$	$-16.7^{+1.2}_{-1.2}$	$-167.2^{+13.9}_{-14.5}$	$-428.3^{+26.4}_{-26.9}$	$280.2^{+24.1}_{-23.7}$
LeoI	$-125.7^{+8.3}_{-9.2}$	$-123.3^{+8.2}_{-9.0}$	$203.4^{+14.9}_{-13.5}$	$-159.1^{+37.6}_{-40.8}$	$-288.2^{+37.7}_{-42.0}$	$100.6^{+26.7}_{-31.4}$
LeoII	$-67.8^{+5.0}_{-4.5}$	$-54.2^{+4.0}_{-3.6}$	$206.9^{+13.8}_{-15.2}$	$22.6^{+33.8}_{-33.5}$	$-196.2^{+36.6}_{-38.6}$	$40.6^{+13.6}_{-14.0}$
LeoIV	$-10.4^{+0.7}_{-0.7}$	$-82.4^{+5.7}_{-5.4}$	$129.9^{+8.5}_{-8.9}$	$-238.1^{+49.6}_{-43.5}$	$-477.0^{+44.9}_{-44.7}$	$-164.6^{+29.9}_{-29.2}$
LeoV	$-15.2^{+1.1}_{-1.1}$	$-89.1^{+6.4}_{-6.4}$	$147.6^{+10.6}_{-10.6}$	$151.9^{+45.5}_{-47.5}$	$-519.5^{+48.6}_{-52.3}$	$-94.6^{+28.5}_{-30.8}$
LMC	$5.2^{+0.4}_{-0.4}$	$-41.5^{+3.0}_{-2.9}$	$-27.3^{+2.0}_{-1.9}$	$-70.9^{+10.2}_{-9.7}$	$-463.3^{+18.5}_{-17.6}$	$210.8^{+25.1}_{-26.2}$
PheII	$31.6^{+2.2}_{-2.1}$	$-23.7^{+1.6}_{-1.7}$	$-69.6^{+4.7}_{-4.9}$	$-46.7^{+42.9}_{-42.6}$	$-467.1^{+61.7}_{-54.3}$	$100.9^{+25.4}_{-27.5}$
PhxI	$-2.6^{+0.2}_{-0.2}$	$-145.8^{+9.7}_{-10.0}$	$-392.7^{+26.0}_{-26.9}$	$-56.8^{+74.8}_{-81.6}$	$-157.1^{+77.8}_{-78.2}$	$81.3^{+29.1}_{-28.8}$
PisII	$26.6^{+1.9}_{-1.8}$	$121.7^{+8.9}_{-8.4}$	$-134.1^{+9.3}_{-9.8}$	$292.8^{+59.0}_{-57.4}$	$-477.9^{+45.3}_{-46.5}$	$-66.5^{+39.6}_{-40.5}$
RetII	$-1.8^{+0.1}_{-0.1}$	$-19.3^{+1.3}_{-1.4}$	$-22.9^{+1.5}_{-1.7}$	$-6.6^{+5.1}_{-4.8}$	$-338.0^{+20.2}_{-22.7}$	$202.9^{+19.1}_{-17.0}$
RetIII	$1.3^{+0.1}_{-0.1}$	$-63.8^{+4.4}_{-4.4}$	$-66.3^{+4.6}_{-4.6}$	$205.7^{+267.3}_{-264.3}$	$-124.9^{+165.1}_{-159.5}$	$-256.3^{+153.7}_{-159.5}$
SgrI	$25.2^{+1.8}_{-1.7}$	$2.2^{+0.2}_{-0.1}$	$-6.2^{+0.4}_{-0.4}$	$217.6^{+6.1}_{-6.0}$	$-270.7^{+19.7}_{-20.4}$	$201.7^{+17.3}_{-16.3}$
SgrII	$58.9^{+4.2}_{-3.7}$	$18.6^{+1.3}_{-1.2}$	$-26.0^{+1.7}_{-1.8}$	$-21.1^{+20.0}_{-18.3}$	$-358.5^{+40.0}_{-45.2}$	$152.4^{+32.2}_{-31.7}$
SclI	$1.7^{+0.1}_{-0.1}$	$-8.0^{+0.5}_{-0.6}$	$-84.4^{+5.5}_{-6.1}$	$2.4^{+14.1}_{-13.9}$	$-73.4^{+14.1}_{-15.3}$	$-104.9^{+1.5}_{-1.4}$
Seg1	$-11.4^{+0.8}_{-0.8}$	$-9.2^{+0.6}_{-0.6}$	$17.7^{+1.2}_{-1.2}$	$-121.5^{+3.4}_{-3.5}$	$-455.0^{+26.1}_{-25.7}$	$-44.1^{+14.3}_{-14.2}$
Seg2	$-24.0^{+1.7}_{-1.7}$	$15.1^{+1.0}_{-1.1}$	$-22.3^{+1.6}_{-1.5}$	$-178.8^{+15.4}_{-15.8}$	$-179.4^{+13.2}_{-13.0}$	$134.9^{+10.5}_{-10.1}$
SMC	$23.1^{+1.6}_{-1.6}$	$-38.1^{+2.6}_{-2.6}$	$-46.0^{+3.1}_{-3.2}$	$-13.4^{+9.2}_{-10.0}$	$-439.1^{+25.0}_{-25.2}$	$154.0^{+18.5}_{-18.8}$
SxtI	$-30.7^{+2.2}_{-2.0}$	$-54.6^{+3.9}_{-3.5}$	$58.5^{+3.8}_{-4.2}$	$-234.7^{+17.3}_{-15.9}$	$-153.3^{+9.9}_{-10.5}$	$62.4^{+11.6}_{-11.4}$
TriII	$-20.8^{+1.4}_{-1.4}$	$17.9^{+1.2}_{-1.2}$	$-12.1^{+0.8}_{-0.8}$	$199.8^{+6.7}_{-6.7}$	$-239.8^{+6.1}_{-6.0}$	$248.0^{+9.1}_{-8.8}$
TucII	$29.0^{+2.0}_{-2.1}$	$-18.2^{+1.3}_{-1.2}$	$-45.6^{+3.4}_{-3.1}$	$-256.5^{+16.0}_{-14.9}$	$-307.9^{+27.4}_{-24.3}$	$121.0^{+6.1}_{-6.6}$
TucIII	$9.5^{+0.7}_{-0.7}$	$-9.6^{+0.7}_{-0.7}$	$-21.0^{+1.5}_{-1.5}$	$16.4^{+5.5}_{-5.3}$	$-121.9^{+11.8}_{-11.8}$	$184.6^{+7.4}_{-7.3}$
UMaI	$-52.5^{+3.5}_{-3.7}$	$21.3^{+1.5}_{-1.4}$	$79.2^{+5.5}_{-5.3}$	$-213.7^{+22.0}_{-22.2}$	$-395.5^{+29.6}_{-31.2}$	$-103.2^{+10.7}_{-10.4}$
UMaII	$-24.2^{+1.5}_{-1.7}$	$13.5^{+1.0}_{-0.8}$	$21.2^{+1.5}_{-1.3}$	$149.7^{+6.4}_{-6.0}$	$-355.5^{+20.7}_{-22.9}$	$204.7^{+19.7}_{-17.9}$
UMiI	$-12.6^{+0.9}_{-0.9}$	$52.6^{+3.6}_{-3.8}$	$53.7^{+3.7}_{-3.8}$	$-9.5^{+5.8}_{-5.8}$	$-197.2^{+4.1}_{-4.1}$	$-156.3^{+3.5}_{-3.5}$
Wil1	$-19.3^{+1.2}_{-1.4}$	$8.2^{+0.6}_{-0.5}$	$32.0^{+2.3}_{-1.9}$	$64.8^{+9.8}_{-8.9}$	$-223.5^{+15.1}_{-18.9}$	$81.4^{+8.9}_{-7.6}$

5 Results

The orbits of the 47 dwarf galaxies were obtained by integrating Eg. (8) for 13.5 Gyr backward. The orbit properties determined for three models of the galactic potential (NFWBB, ASBB and ASI) are listed in Table 4. The comparison of the properties obtained for these models of the galactic potential with different masses is illustrated in Figs. 3 and 4. The orbits of the dwarfs integrated in NFWBB, ASBB and ASI models of the galactic potential are shown in Figs. 5, 6 and 7 respectively.

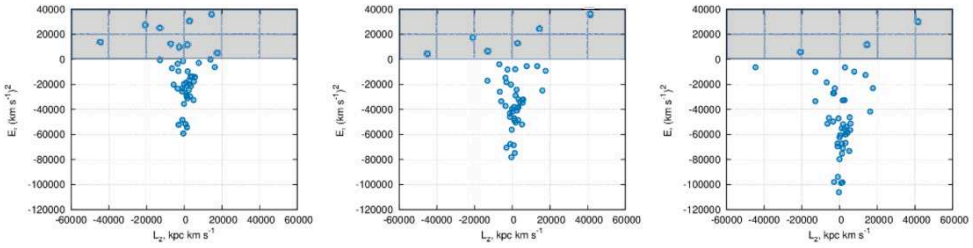


Figure 3 "L_Z–E" diagrams for three models of the galactic gravitational potential: the NFWBB (left-hand panel), the ASBB (middle panel) and the ASI (right-hand panel).

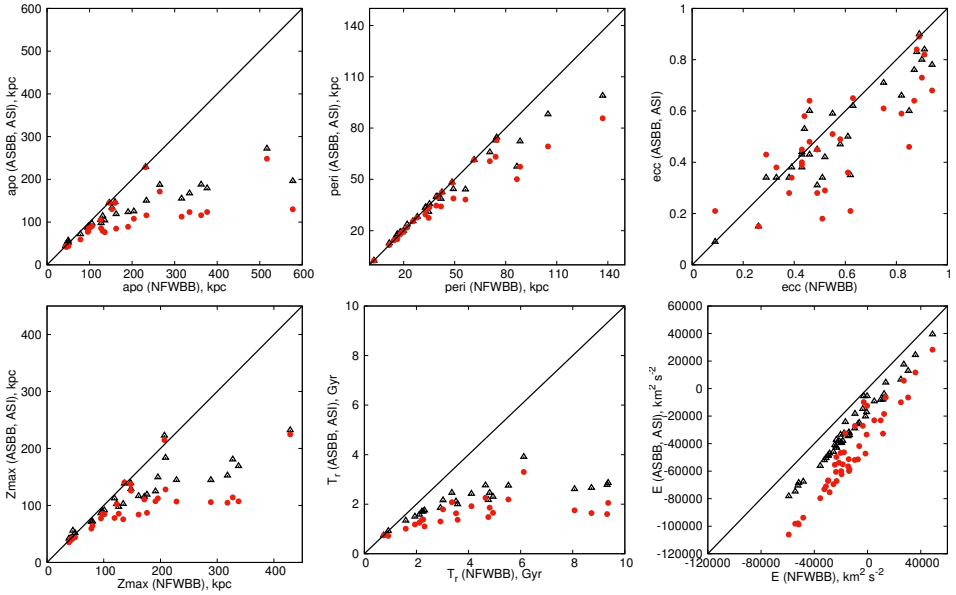


Figure 4 Comparison of the orbital parameters (apo, peri, ecc, Z_{max}, T_r and E) obtained in NFWBB, ASBB and ASI axisymmetric potentials. The parameters obtained in the ASBB (black triangles) and the ASI (red dots) models of the galactic potential are compared with corresponding orbit parameters obtained in the NFWBB model. In each panel we plot the line of coincidence.

Table 4 Dwarf orbital properties. For each dwarf we quote values derived from orbits integrated for 13.5 Gyr backward in three potentials of models NFWBB, ASBB and ASI in the first, second, and third row, respectively.

Name	d_{GC} [kpc]	Π [km/s]	Θ [km/s]	V_{tot} [km/s]	apo [kpc]	peri [kpc]	ecc	incl. θ [deg]	T_r [Gyr]	L_Z [kpc km/s]	E [(km/s)^2]
AquII	105	266^{+30}_{-31}	-43^{+26}_{-31}	299^{+30}_{-28}	–	–	–	–	–	−2629	9873
	106	261^{+26}_{-26}	-41^{+40}_{-39}	295^{+29}_{-20}	682^{+0}_{-725}	103^{+17}_{-25}	$0.74^{+0.26}_{-0.13}$	$94.7^{+4.5}_{-4.2}$	$18.70^{+0.00}_{-20.14}$	−2483	−8157
	106	264^{+25}_{-31}	-42^{+32}_{-28}	297^{+27}_{-27}	280^{+201}_{-125}	103^{+6}_{-7}	$0.46^{+0.20}_{-0.14}$	$94.7^{+3.6}_{-3.3}$	$5.04^{+5.63}_{-3.01}$	−2548	−23102
BooI	64	126^{+13}_{-11}	118^{+30}_{-22}	185^{+24}_{-16}	97^{+30}_{-14}	39^{+9}_{-8}	$0.43^{+0.06}_{-0.02}$	$80.2^{+2.0}_{-1.7}$	$2.04^{+0.78}_{-0.40}$	1741	−31258
	64	127^{+12}_{-13}	122^{+24}_{-29}	188^{+20}_{-22}	88^{+16}_{-10}	40^{+8}_{-8}	$0.38^{+0.06}_{-0.03}$	$80.0^{+1.4}_{-2.0}$	$1.60^{+0.30}_{-0.23}$	1814	−50438
	64	126^{+11}_{-11}	119^{+29}_{-29}	186^{+22}_{-18}	78^{+8}_{-5}	35^{+8}_{-7}	$0.39^{+0.07}_{-0.06}$	$80.2^{+1.7}_{-2.1}$	$1.25^{+0.16}_{-0.13}$	1756	−71036
BooII	39	-307^{+30}_{-25}	244^{+40}_{-30}	392^{+30}_{-25}	–	–	–	–	–	1637	11583
	39	-305^{+33}_{-29}	248^{+28}_{-29}	394^{+26}_{-26}	–	–	–	–	–	1669	−7932
	39	-305^{+36}_{-26}	247^{+33}_{-33}	393^{+23}_{-27}	234^{+143}_{-88}	39^{+5}_{-7}	$0.72^{+0.08}_{-0.09}$	$83.8^{+0.8}_{-1.0}$	$3.29^{+3.41}_{-1.85}$	1635	−32754
BooIII	49	-66^{+26}_{-40}	-7^{+24}_{-21}	274^{+16}_{-5}	234^{+144}_{-121}	12^{+6}_{-3}	$0.91^{+0.05}_{-0.04}$	$90.5^{+2.1}_{-2.0}$	$4.64^{+4.18}_{-2.89}$	−53	−19518
	49	-71^{+25}_{-30}	-6^{+22}_{-26}	275^{+17}_{-6}	150^{+86}_{-60}	13^{+5}_{-3}	$0.84^{+0.07}_{-0.03}$	$90.5^{+1.7}_{-1.9}$	$2.18^{+0.79}_{-0.65}$	−42	−39549
	49	-68^{+25}_{-33}	-7^{+24}_{-23}	274^{+16}_{-7}	116^{+70}_{-51}	12^{+4}_{-3}	$0.82^{+0.07}_{-0.05}$	$90.5^{+1.9}_{-2.0}$	$1.48^{+0.32}_{-0.31}$	−55	−62243
CVenI	212	110^{+28}_{-38}	-84^{+35}_{-28}	154^{+26}_{-28}	517^{+0}_{-442}	137^{+28}_{-44}	$0.58^{+0.33}_{-0.08}$	$96.4^{+2.2}_{-2.1}$	$16.82^{+0.00}_{-13.69}$	−3022	−9436
	212	105^{+41}_{-27}	-84^{+32}_{-34}	150^{+41}_{-21}	272^{+139}_{-93}	99^{+47}_{-25}	$0.47^{+0.20}_{-0.08}$	$96.6^{+2.3}_{-1.5}$	$5.50^{+5.01}_{-2.42}$	−3008	−18295
	209	108^{+32}_{-36}	-84^{+34}_{-34}	153^{+34}_{-27}	248^{+73}_{-45}	86^{+37}_{-30}	$0.49^{+0.12}_{-0.09}$	$96.4^{+1.9}_{-2.0}$	$4.09^{+2.64}_{-1.52}$	−3005	−27067
CVenII	163	-144^{+46}_{-47}	-138^{+46}_{-40}	211^{+51}_{-47}	–	–	–	–	–	−3416	−3575
	161	-147^{+46}_{-48}	-141^{+46}_{-53}	216^{+58}_{-44}	319^{+77}_{-282}	126^{+0}_{-113}	$0.43^{+0.49}_{-0.08}$	$96.4^{+1.6}_{-1.4}$	$7.45^{+2.39}_{-7.26}$	−3494	−14728
	162	-145^{+50}_{-49}	-140^{+57}_{-35}	213^{+48}_{-53}	222^{+125}_{-123}	114^{+15}_{-70}	$0.32^{+0.38}_{-0.05}$	$96.4^{+1.8}_{-1.0}$	$3.92^{+3.54}_{-2.96}$	−3466	−27017
CarI	104	55^{+9}_{-9}	36^{+19}_{-12}	164^{+20}_{-21}	126^{+97}_{-54}	105^{+8}_{-32}	$0.09^{+0.26}_{-0.07}$	$78.1^{+6.4}_{-3.7}$	$4.05^{+2.72}_{-1.91}$	3568	−21443
	104	59^{+13}_{-8}	35^{+15}_{-17}	165^{+22}_{-16}	105^{+15}_{-6}	88^{+14}_{-17}	$0.09^{+0.11}_{-0.04}$	$78.7^{+4.6}_{-5.5}$	$2.43^{+0.34}_{-0.26}$	3418	−38049
	106	57^{+8}_{-11}	36^{+14}_{-18}	165^{+18}_{-20}	105^{+8}_{-5}	69^{+14}_{-14}	$0.21^{+0.10}_{-0.09}$	$78.3^{+5.1}_{-6.0}$	$1.92^{+0.20}_{-0.18}$	3506	−53875
CarII	38	251^{+8}_{-8}	-178^{+8}_{-13}	346^{+12}_{-10}	853^{+0}_{-878}	28^{+2}_{-2}	$0.94^{+0.06}_{-0.03}$	$127.3^{+2.4}_{-3.3}$	$26.25^{+0.00}_{-27.14}$	−6451	−7199
	37	256^{+7}_{-9}	-180^{+11}_{-11}	350^{+13}_{-9}	232^{+59}_{-35}	28^{+2}_{-2}	$0.78^{+0.03}_{-0.02}$	$127.3^{+3.1}_{-2.3}$	$3.60^{+1.30}_{-0.67}$	−6502	−25884
	38	252^{+7}_{-8}	-179^{+10}_{-10}	348^{+12}_{-11}	145^{+21}_{-14}	28^{+2}_{-2}	$0.68^{+0.02}_{-0.02}$	$127.4^{+2.8}_{-3.2}$	$1.97^{+0.27}_{-0.18}$	−6500	−51419
CarIII	29	142^{+7}_{-11}	-21^{+8}_{-8}	389^{+33}_{-23}	–	–	–	–	–	−602	−1531
	29	147^{+8}_{-10}	-23^{+8}_{-8}	391^{+29}_{-27}	298^{+135}_{-217}	29^{+1}_{-2}	$0.82^{+0.11}_{-0.08}$	$93.3^{+1.1}_{-1.2}$	$5.04^{+4.01}_{-4.60}$	−650	−20224
	29	144^{+9}_{-7}	-22^{+9}_{-8}	390^{+29}_{-30}	161^{+90}_{-62}	29^{+2}_{-2}	$0.69^{+0.08}_{-0.09}$	$93.2^{+1.3}_{-1.1}$	$2.19^{+1.66}_{-1.09}$	−635	−47186

Table 4 (continued)

Name	d_{GC} [kpc]	Π [km/s]	Θ [km/s]	V_{tot} [km/s]	apo [kpc]	peri [kpc]	ecc	incl. θ [deg]	T_r [Gyr]	L_Z [kpc km/s]	E [(km/s)^2]
CBerI	43	-233^{+16}_{-18}	-95^{+18}_{-21}	268^{+19}_{-15}	136^{+87}_{-45}	43^{+3}_{-2}	$0.52^{+0.13}_{-0.09}$	$95.4^{+1.0}_{-1.1}$	$2.91^{+2.25}_{-1.12}$	-1075	-25626
	43	-231^{+18}_{-19}	-99^{+19}_{-20}	268^{+18}_{-15}	104^{+27}_{-18}	43^{+3}_{-2}	$0.42^{+0.08}_{-0.06}$	$95.6^{+1.1}_{-1.1}$	$1.85^{+0.39}_{-0.27}$	-1127	-45916
	43	-232^{+13}_{-20}	-96^{+19}_{-20}	268^{+19}_{-12}	76^{+17}_{-10}	42^{+2}_{-3}	$0.29^{+0.07}_{-0.05}$	$95.5^{+1.1}_{-1.0}$	$1.30^{+0.22}_{-0.14}$	-1096	-69489
ColI	188	-34^{+193}_{-167}	-269^{+214}_{-153}	272^{+227}_{-44}	–	–	–	–	–	-44403	13687
	188	-31^{+200}_{-199}	-273^{+186}_{-234}	275^{+315}_{-28}	–	–	–	–	–	-44946	4369
	187	-33^{+189}_{-185}	-271^{+175}_{-217}	273^{+291}_{-26}	–	–	–	–	–	-44629	-6363
CraI	144	-74^{+37}_{-34}	-36^{+42}_{-44}	94^{+45}_{-22}	146^{+57}_{-22}	56^{+50}_{-24}	$0.44^{+0.21}_{-0.21}$	$104.7^{+16.3}_{-14.5}$	$3.43^{+2.45}_{-0.86}$	-3436	-23427
	145	-69^{+31}_{-39}	-37^{+51}_{-39}	91^{+46}_{-18}	145^{+14}_{-6}	44^{+36}_{-19}	$0.53^{+0.17}_{-0.22}$	$105.3^{+21.2}_{-12.3}$	$2.43^{+0.52}_{-0.19}$	-3460	-37226
	145	-72^{+31}_{-34}	-36^{+44}_{-41}	93^{+42}_{-10}	145^{+13}_{-7}	38^{+28}_{-11}	$0.58^{+0.10}_{-0.19}$	$104.9^{+16.8}_{-13.1}$	$2.08^{+0.35}_{-0.11}$	-3438	-49697
CraII	117	-122^{+14}_{-15}	30^{+21}_{-19}	126^{+18}_{-11}	153^{+28}_{-15}	35^{+12}_{-8}	$0.63^{+0.08}_{-0.08}$	$76.0^{+8.9}_{-8.8}$	$3.13^{+0.80}_{-0.38}$	2528	-24555
	116	-117^{+15}_{-14}	30^{+18}_{-19}	121^{+16}_{-13}	134^{+8}_{-9}	31^{+9}_{-7}	$0.62^{+0.08}_{-0.08}$	$75.3^{+8.4}_{-9.5}$	$2.14^{+0.16}_{-0.16}$	2568	-40971
	115	-120^{+14}_{-18}	30^{+19}_{-20}	124^{+21}_{-12}	130^{+8}_{-8}	28^{+9}_{-7}	$0.65^{+0.07}_{-0.09}$	$75.7^{+8.0}_{-9.6}$	$1.79^{+0.15}_{-0.12}$	2555	-55354
DraI	79	6^{+6}_{-8}	48^{+14}_{-11}	159^{+11}_{-10}	106^{+13}_{-10}	42^{+6}_{-7}	$0.43^{+0.06}_{-0.03}$	$73.4^{+4.6}_{-3.4}$	$2.26^{+0.37}_{-0.31}$	3122	-29515
	80	1^{+5}_{-8}	48^{+12}_{-16}	159^{+12}_{-11}	97^{+8}_{-5}	39^{+6}_{-5}	$0.43^{+0.05}_{-0.05}$	$73.0^{+4.0}_{-5.4}$	$1.70^{+0.16}_{-0.10}$	3110	-48412
	79	4^{+7}_{-8}	48^{+12}_{-10}	159^{+14}_{-10}	90^{+6}_{-5}	34^{+5}_{-4}	$0.45^{+0.04}_{-0.04}$	$73.1^{+4.0}_{-3.4}$	$1.38^{+0.11}_{-0.08}$	3118	-66704
DraII	22	69^{+7}_{-8}	72^{+6}_{-8}	348^{+7}_{-9}	131^{+25}_{-27}	19^{+1}_{-1}	$0.75^{+0.02}_{-0.05}$	$79.6^{+0.9}_{-1.0}$	$2.37^{+0.58}_{-0.60}$	1272	-28537
	22	65^{+7}_{-6}	69^{+7}_{-7}	347^{+10}_{-8}	114^{+16}_{-10}	19^{+1}_{-1}	$0.71^{+0.03}_{-0.02}$	$79.9^{+1.0}_{-1.0}$	$1.73^{+0.23}_{-0.14}$	1223	-47113
	22	68^{+7}_{-8}	71^{+6}_{-7}	348^{+7}_{-10}	79^{+6}_{-8}	19^{+1}_{-1}	$0.61^{+0.03}_{-0.03}$	$79.6^{+0.9}_{-1.0}$	$1.10^{+0.07}_{-0.10}$	1263	-75272
EriII	364	-37^{+80}_{-80}	770^{+86}_{-89}	772^{+90}_{-80}	–	–	–	–	–	175224	283935
	366	-33^{+96}_{-85}	768^{+78}_{-98}	770^{+84}_{-89}	–	–	–	–	–	174746	279188
	365	-35^{+64}_{-77}	769^{+83}_{-112}	771^{+86}_{-102}	–	–	–	–	–	175075	275003
FnxI	141	57^{+28}_{-23}	-89^{+30}_{-28}	128^{+32}_{-24}	160^{+83}_{-36}	88^{+37}_{-35}	$0.29^{+0.24}_{-0.09}$	$108.9^{+4.6}_{-3.1}$	$4.48^{+2.98}_{-1.53}$	-5561	-20238
	142	61^{+31}_{-26}	-93^{+22}_{-34}	132^{+36}_{-16}	147^{+23}_{-11}	72^{+39}_{-18}	$0.34^{+0.13}_{-0.18}$	$108.9^{+3.4}_{-3.1}$	$2.79^{+0.75}_{-0.31}$	-5768	-33514
	140	58^{+30}_{-26}	-91^{+31}_{-22}	130^{+26}_{-23}	145^{+9}_{-10}	57^{+23}_{-20}	$0.43^{+0.15}_{-0.14}$	$108.9^{+4.9}_{-2.9}$	$2.26^{+0.28}_{-0.24}$	-5652	-46767
GruI	116	57^{+26}_{-28}	-128^{+31}_{-24}	300^{+21}_{-16}	–	–	–	–	–	-7043	12422
	116	59^{+20}_{-30}	-123^{+20}_{-22}	299^{+13}_{-18}	–	–	–	–	–	-6800	-3914
	116	58^{+26}_{-30}	-126^{+35}_{-27}	299^{+21}_{-16}	400^{+188}_{-186}	69^{+12}_{-43}	$0.71^{+0.18}_{-0.08}$	$106.0^{+3.7}_{-2.7}$	$7.27^{+5.07}_{-4.15}$	-6940	-18450

©2021 Astronomical and Astrophysical Transactions (AApTr), Vol. 32, Issue 3

Table 4 (continued)

Name	d_{GC} [kpc]	Π [km/s]	Θ [km/s]	V_{tot} [km/s]	apo [kpc]	peri [kpc]	ecc	incl. θ [deg]	T_r [Gyr]	L_Z [kpc km/s]	E [(km/s)^2]
HerI	128	110^{+19}_{-19}	51^{+32}_{-24}	159^{+22}_{-13}	265^{+118}_{-62}	16^{+17}_{-7}	$0.88^{+0.06}_{-0.09}$	$40.4^{+5.3}_{-17.9}$	$5.54^{+3.82}_{-1.83}$	5145	−17683
	130	107^{+22}_{-21}	55^{+27}_{-24}	159^{+21}_{-12}	187^{+27}_{-16}	18^{+15}_{-9}	$0.83^{+0.07}_{-0.13}$	$40.6^{+3.8}_{-11.1}$	$2.75^{+0.48}_{-0.21}$	5574	−32521
	130	109^{+20}_{-21}	53^{+26}_{-27}	159^{+19}_{-13}	172^{+27}_{-29}	15^{+12}_{-8}	$0.84^{+0.08}_{-0.11}$	$40.5^{+4.3}_{-15.6}$	$2.19^{+0.30}_{-0.23}$	5312	−46313
HorI	80	131^{+30}_{-28}	5^{+17}_{-25}	191^{+26}_{-21}	127^{+118}_{-52}	74^{+9}_{-16}	$0.26^{+0.23}_{-0.07}$	$89.1^{+3.2}_{-4.5}$	$3.38^{+3.27}_{-1.59}$	223	−23692
	79	136^{+25}_{-28}	4^{+24}_{-22}	195^{+22}_{-18}	98^{+93}_{-67}	73^{+8}_{-18}	$0.15^{+0.20}_{-0.07}$	$89.3^{+4.4}_{-4.0}$	$2.14^{+2.64}_{-2.14}$	181	−41894
	79	133^{+24}_{-30}	4^{+18}_{-27}	193^{+22}_{-20}	86^{+21}_{-11}	63^{+9}_{-13}	$0.15^{+0.14}_{-0.06}$	$89.3^{+3.4}_{-4.9}$	$1.63^{+0.24}_{-0.22}$	194	−60536
HorII	77	319^{+106}_{-91}	62^{+145}_{-113}	383^{+129}_{-57}	–	–	–	–	–	2876	30483
	78	324^{+101}_{-74}	60^{+139}_{-90}	387^{+116}_{-51}	–	–	–	–	–	2801	12872
	77	321^{+99}_{-95}	61^{+98}_{-136}	384^{+108}_{-65}	–	–	–	–	–	2819	−6486
HyaII	132	11^{+33}_{-19}	160^{+28}_{-49}	264^{+25}_{-28}	–	–	–	–	–	17561	5052
	133	16^{+26}_{-29}	161^{+38}_{-39}	266^{+40}_{-35}	593^{+0}_{-590}	105^{+14}_{-16}	$0.70^{+0.28}_{-0.17}$	$54.5^{+5.0}_{-6.0}$	$15.53^{+0.00}_{-15.78}$	17744	−9216
	133	13^{+29}_{-26}	160^{+29}_{-37}	265^{+32}_{-24}	283^{+238}_{-114}	101^{+13}_{-16}	$0.47^{+0.21}_{-0.07}$	$54.8^{+4.4}_{-6.6}$	$5.07^{+6.94}_{-3.10}$	17626	−23038
HyiI	26	163^{+28}_{-27}	166^{+18}_{-13}	370^{+22}_{-21}	362^{+113}_{-312}	26^{+3}_{-22}	$0.87^{+0.12}_{-0.09}$	$69.6^{+2.6}_{-2.0}$	$8.49^{+3.90}_{-8.04}$	3301	−13882
	26	168^{+28}_{-29}	166^{+16}_{-11}	372^{+25}_{-20}	188^{+106}_{-55}	26^{+1}_{-1}	$0.76^{+0.07}_{-0.06}$	$69.73^{+2.4}_{-1.8}$	$2.83^{+2.33}_{-1.09}$	3306	−31903
	26	165^{+28}_{-32}	165^{+16}_{-12}	371^{+23}_{-15}	116^{+37}_{-19}	26^{+1}_{-2}	$0.64^{+0.07}_{-0.04}$	$69.8^{+2.2}_{-2.0}$	$1.60^{+0.46}_{-0.23}$	3285	−59919
LeoI	272	131^{+47}_{-38}	77^{+42}_{-46}	186^{+47}_{-25}	–	–	–	–	–	13957	−323
	274	134^{+39}_{-47}	73^{+48}_{-22}	187^{+45}_{-26}	–	–	–	–	–	13301	−5430
	275	132^{+41}_{-32}	75^{+43}_{-40}	186^{+44}_{-20}	620^{+114}_{-533}	53^{+44}_{-18}	$0.84^{+0.15}_{-0.06}$	$51.0^{+6.5}_{-19.3}$	$12.95^{+3.52}_{-10.24}$	13699	−12571
LeoII	229	-62^{+36}_{-29}	29^{+31}_{-39}	84^{+32}_{-17}	232^{+61}_{-21}	87^{+77}_{-42}	$0.46^{+0.22}_{-0.24}$	$81.5^{+8.4}_{-11.3}$	$6.28^{+3.61}_{-1.25}$	2735	−16671
	229	-59^{+42}_{-23}	25^{+39}_{-36}	80^{+31}_{-20}	229^{+18}_{-11}	58^{+39}_{-28}	$0.60^{+0.17}_{-0.19}$	$82.3^{+10.5}_{-10.7}$	$3.88^{+0.68}_{-0.32}$	2362	−24281
	228	-61^{+38}_{-42}	28^{+31}_{-39}	82^{+41}_{-16}	228^{+56}_{-39}	50^{+43}_{-20}	$0.64^{+0.12}_{-0.21}$	$81.8^{+7.8}_{-12.3}$	$3.30^{+1.55}_{-0.85}$	2596	−32572
LeoIV	153	266^{+42}_{-46}	173^{+43}_{-36}	354^{+43}_{-35}	–	–	–	–	–	14589	35941
	155	270^{+34}_{-56}	172^{+45}_{-55}	357^{+39}_{-51}	–	–	–	–	–	14498	24405
	155	268^{+30}_{-58}	172^{+38}_{-46}	355^{+31}_{-50}	–	–	–	–	–	14532	11689
LeoV	174	213^{+50}_{-45}	-225^{+46}_{-52}	322^{+54}_{-39}	–	–	–	–	–	−20697	27287
	175	218^{+39}_{-56}	-226^{+49}_{-59}	326^{+50}_{-44}	–	–	–	–	–	−20812	17495
	173	215^{+43}_{-55}	-225^{+49}_{-54}	323^{+51}_{-45}	–	–	–	–	–	−20768	5753

©2021 Astronomical and Astrophysical Transactions (AApTr), Vol. 32, Issue 3

Table 4 (continued)

Name	d_{GC} [kpc]	Π [km/s]	Θ [km/s]	V_{tot} [km/s]	apo [kpc]	peri [kpc]	ecc	incl. θ [deg]	T_r [Gyr]	L_Z [kpc km/s]	E [(km/s)^2]
LMC	50	211^{+18}_{-18}	44^{+12}_{-9}	307^{+21}_{-17}	578^{+0}_{-587}	49^{+5}_{-6}	$0.85^{+0.15}_{-0.11}$	$82.9^{+2.0}_{-1.5}$	$16.20^{+0.00}_{-16.92}$	1846	−9574
	50	216^{+21}_{-16}	44^{+8}_{-11}	310^{+25}_{-21}	196^{+95}_{-59}	48^{+2}_{-3}	$0.60^{+0.11}_{-0.07}$	$83.1^{+1.5}_{-1.9}$	$3.18^{+2.19}_{-1.17}$	1831	−28870
	50	213^{+20}_{-21}	44^{+9}_{-10}	308^{+25}_{-23}	130^{+37}_{-25}	48^{+2}_{-3}	$0.46^{+0.09}_{-0.07}$	$83.1^{+1.8}_{-1.7}$	$1.99^{+0.46}_{-0.32}$	1819	−51851
PheII	77	126^{+51}_{-54}	173^{+64}_{-37}	240^{+69}_{-38}	316^{+86}_{-344}	75^{+0}_{-76}	$0.62^{+0.42}_{-0.16}$	$71.6^{+4.2}_{-3.3}$	$8.36^{+3.18}_{-9.53}$	5749	−14111
	76	129^{+47}_{-54}	176^{+60}_{-39}	244^{+63}_{-42}	155^{+134}_{-91}	75^{+10}_{-27}	$0.35^{+0.33}_{-0.11}$	$71.6^{+3.8}_{-2.5}$	$2.92^{+3.02}_{-1.94}$	5862	−32074
	77	128^{+57}_{-56}	174^{+56}_{-46}	241^{+66}_{-40}	113^{+151}_{-58}	73^{+7}_{-21}	$0.21^{+0.30}_{-0.03}$	$71.6^{+3.5}_{-3.9}$	$2.05^{+2.90}_{-1.43}$	5771	−51261
PhxI	423	-95^{+69}_{-73}	53^{+71}_{-89}	141^{+78}_{-18}	–	–	–	–	–	7744	−2847
	423	-90^{+79}_{-74}	53^{+70}_{-74}	137^{+82}_{-26}	–	–	–	–	–	7691	−5512
	421	-93^{+75}_{-81}	53^{+66}_{-85}	139^{+87}_{-36}	–	–	–	–	–	7733	−9814
PisII	182	-174^{+33}_{-57}	333^{+49}_{-62}	381^{+58}_{-46}	–	–	–	–	–	41039	48805
	183	-179^{+47}_{-46}	334^{+68}_{-58}	384^{+66}_{-45}	–	–	–	–	–	41128	39436
	182	-176^{+38}_{-58}	334^{+53}_{-49}	382^{+63}_{-38}	–	–	–	–	–	41051	28240
RetII	32	70^{+19}_{-19}	-42^{+11}_{-12}	226^{+21}_{-18}	50^{+13}_{-8}	22^{+3}_{-3}	$0.39^{+0.10}_{-0.05}$	$98.3^{+1.9}_{-1.8}$	$0.91^{+0.24}_{-0.16}$	−914	−48332
	32	75^{+16}_{-18}	-44^{+11}_{-9}	227^{+16}_{-16}	52^{+10}_{-7}	24^{+2}_{-3}	$0.38^{+0.07}_{-0.06}$	$98.6^{+1.9}_{-1.4}$	$0.93^{+0.14}_{-0.10}$	−963	−67592
	32	72^{+19}_{-18}	-43^{+12}_{-10}	226^{+23}_{-19}	45^{+7}_{-5}	22^{+3}_{-3}	$0.34^{+0.08}_{-0.05}$	$98.5^{+1.9}_{-1.5}$	$0.72^{+0.10}_{-0.07}$	−941	−93834
RetIII	94	-154^{+181}_{-166}	-201^{+298}_{-167}	355^{+219}_{-83}	–	–	–	–	–	−12922	25054
	92	-149^{+156}_{-169}	-202^{+290}_{-267}	354^{+310}_{-40}	–	–	–	–	–	−12956	6557
	91	-152^{+153}_{-174}	-201^{+281}_{-256}	355^{+319}_{-48}	753^{+0}_{-819}	89^{+6}_{-63}	$0.79^{+0.32}_{-0.15}$	$113.8^{+31.7}_{-13.7}$	$18.20^{+0.00}_{-19.55}$	−12923	−9954
SgrI	18	225^{+6}_{-8}	44^{+22}_{-15}	310^{+12}_{-10}	50^{+12}_{-11}	14^{+1}_{-1}	$0.55^{+0.05}_{-0.05}$	$81.4^{+4.1}_{-2.9}$	$0.79^{+0.22}_{-0.18}$	746	−51706
	18	224^{+6}_{-7}	49^{+17}_{-21}	310^{+11}_{-12}	57^{+12}_{-11}	15^{+1}_{-1}	$0.59^{+0.06}_{-0.05}$	$80.5^{+3.4}_{-4.1}$	$0.89^{+0.16}_{-0.16}$	829	−68513
	18	225^{+6}_{-8}	46^{+21}_{-18}	310^{+9}_{-10}	44^{+7}_{-8}	14^{+1}_{-1}	$0.51^{+0.06}_{-0.06}$	$81.0^{+4.2}_{-3.4}$	$0.63^{+0.08}_{-0.10}$	777	−98704
SgrII	60	-45^{+22}_{-26}	93^{+41}_{-34}	190^{+36}_{-29}	96^{+65}_{-30}	33^{+9}_{-8}	$0.49^{+0.13}_{-0.06}$	$57.5^{+12.9}_{-11.0}$	$1.89^{+1.65}_{-0.79}$	4989	−32506
	60	-46^{+22}_{-21}	97^{+36}_{-41}	193^{+36}_{-28}	87^{+29}_{-14}	34^{+8}_{-7}	$0.45^{+0.10}_{-0.06}$	$56.2^{+10.6}_{-13.5}$	$1.52^{+0.46}_{-0.26}$	5237	−52009
	60	-45^{+27}_{-24}	94^{+40}_{-44}	191^{+37}_{-31}	77^{+17}_{-9}	30^{+8}_{-6}	$0.45^{+0.09}_{-0.07}$	$57.0^{+11.4}_{-14.6}$	$1.18^{+0.26}_{-0.16}$	5075	−73168
SclI	84	-150^{+16}_{-17}	106^{+18}_{-14}	208^{+15}_{-11}	204^{+103}_{-59}	71^{+6}_{-7}	$0.49^{+0.09}_{-0.07}$	$86.2^{+0.6}_{-0.5}$	$5.16^{+3.13}_{-1.77}$	1097	−18618
	85	-146^{+17}_{-16}	103^{+16}_{-15}	203^{+14}_{-12}	125^{+18}_{-12}	66^{+7}_{-7}	$0.31^{+0.03}_{-0.00}$	$86.2^{+0.5}_{-0.5}$	$2.42^{+0.31}_{-0.25}$	1065	−37934
	85	-147^{+14}_{-15}	106^{+13}_{-17}	206^{+13}_{-13}	108^{+10}_{-9}	61^{+6}_{-7}	$0.28^{+0.03}_{-0.02}$	$86.1^{+0.4}_{-0.5}$	$1.86^{+0.17}_{-0.17}$	1103	−55036

©2021 Astronomical and Astrophysical Transactions (AApTr), Vol. 32, Issue 3

Table 4 (continued)

Name	d_{GC} [kpc]	Π [km/s]	Θ [km/s]	V_{tot} [km/s]	apo [kpc]	peri [kpc]	ecc	incl. θ [deg]	T_r [Gyr]	L_Z [kpc km/s]	E [(km/s)^2]
Seg1	28	184^{+12}_{-13}	-133^{+25}_{-24}	230^{+23}_{-22}	46^{+12}_{-8}	18^{+3}_{-2}	$0.43^{+0.07}_{-0.04}$	$121.6^{+4.4}_{-3.2}$	$0.78^{+0.22}_{-0.15}$	-2900	-52276
	28	186^{+12}_{-14}	-138^{+26}_{-23}	235^{+23}_{-25}	50^{+12}_{-9}	19^{+2}_{-3}	$0.44^{+0.07}_{-0.04}$	$122.1^{+4.1}_{-3.1}$	$0.84^{+0.18}_{-0.14}$	-2997	-70512
	28	185^{+14}_{-11}	-135^{+21}_{-25}	232^{+26}_{-19}	42^{+8}_{-4}	18^{+3}_{-2}	$0.40^{+0.06}_{-0.03}$	$122.0^{+3.5}_{-3.6}$	$0.65^{+0.11}_{-0.07}$	-2958	-97922
Seg2	42	184^{+16}_{-15}	-1^{+17}_{-16}	233^{+14}_{-13}	79^{+20}_{-20}	35^{+2}_{-3}	$0.38^{+0.14}_{-0.10}$	$90.37^{+3.9}_{-3.5}$	$1.61^{+0.37}_{-0.37}$	-46	-35557
	42	182^{+15}_{-13}	-6^{+17}_{-14}	231^{+14}_{-10}	72^{+17}_{-18}	36^{+2}_{-2}	$0.34^{+0.17}_{-0.11}$	$91.3^{+3.9}_{-3.0}$	$1.33^{+0.25}_{-0.26}$	-204	-56221
	42	184^{+17}_{-13}	-3^{+15}_{-14}	232^{+15}_{-11}	59^{+56}_{-43}	34^{+2}_{-3}	$0.28^{+0.25}_{-0.12}$	$90.6^{+3.4}_{-3.3}$	$1.01^{+0.71}_{-0.60}$	-100	-79686
SMC	62	170^{+18}_{-26}	68^{+11}_{-16}	244^{+19}_{-26}	191^{+106}_{-98}	61^{+5}_{-8}	$0.51^{+0.17}_{-0.20}$	$79.2^{+1.8}_{-2.3}$	$4.60^{+3.04}_{-2.52}$	2796	-19852
	61	174^{+23}_{-25}	70^{+18}_{-14}	248^{+21}_{-24}	123^{+31}_{-30}	61^{+2}_{-4}	$0.34^{+0.10}_{-0.12}$	$79.1^{+2.9}_{-1.8}$	$2.34^{+0.42}_{-0.43}$	2869	-38890
	61	172^{+24}_{-24}	69^{+14}_{-15}	245^{+24}_{-23}	89^{+26}_{-18}	61^{+3}_{-5}	$0.18^{+0.12}_{-0.07}$	$79.3^{+2.0}_{-2.2}$	$1.65^{+0.30}_{-0.23}$	2806	-60004
SxtI	89	46^{+15}_{-21}	242^{+13}_{-18}	256^{+15}_{-19}	–	–	–	–	–	16224	-6275
	89	50^{+13}_{-21}	239^{+16}_{-12}	254^{+17}_{-12}	207^{+59}_{-31}	80^{+5}_{-4}	$0.44^{+0.09}_{-0.05}$	$41.3^{+2.6}_{-1.9}$	$3.71^{+1.38}_{-0.60}$	16033	-24883
	89	48^{+17}_{-16}	241^{+14}_{-16}	255^{+15}_{-16}	154^{+24}_{-21}	78^{+5}_{-5}	$0.33^{+0.06}_{-0.06}$	$41.3^{+2.2}_{-2.6}$	$2.58^{+0.30}_{-0.29}$	16160	-41783
TriII	36	-171^{+8}_{-7}	124^{+9}_{-9}	331^{+9}_{-7}	376^{+146}_{-105}	20^{+4}_{-11}	$0.90^{+0.05}_{-0.03}$	$58.1^{+1.9}_{-2.3}$	$8.79^{+4.57}_{-2.89}$	4246	-13590
	36	-174^{+10}_{-8}	120^{+9}_{-9}	331^{+8}_{-10}	179^{+19}_{-21}	20^{+1}_{-2}	$0.80^{+0.02}_{-0.02}$	$58.8^{+2.2}_{-1.9}$	$2.66^{+0.28}_{-0.32}$	4104	-33709
	37	-172^{+9}_{-9}	122^{+10}_{-8}	331^{+9}_{-8}	124^{+12}_{-9}	20^{+2}_{-1}	$0.73^{+0.02}_{-0.02}$	$58.4^{+2.2}_{-2.0}$	$1.64^{+0.16}_{-0.11}$	4192	-58542
TucII	53	-150^{+28}_{-22}	201^{+26}_{-22}	282^{+16}_{-13}	335^{+189}_{-162}	33^{+6}_{-20}	$0.82^{+0.11}_{-0.06}$	$60.4^{+2.5}_{-2.3}$	$7.85^{+6.22}_{-4.59}$	5530	-14538
	53	-147^{+23}_{-22}	204^{+25}_{-18}	283^{+17}_{-10}	167^{+37}_{-19}	34^{+4}_{-3}	$0.66^{+0.04}_{-0.02}$	$60.2^{+2.6}_{-2.5}$	$2.63^{+0.61}_{-0.34}$	5631	-34531
	54	-149^{+23}_{-22}	203^{+26}_{-19}	282^{+17}_{-10}	124^{+21}_{-10}	32^{+5}_{-3}	$0.59^{+0.04}_{-0.02}$	$60.4^{+2.8}_{-2.2}$	$1.75^{+0.29}_{-0.14}$	5564	-56511
TucIII	23	-130^{+10}_{-13}	-44^{+11}_{-10}	236^{+10}_{-8}	46^{+6}_{-5}	3^{+1}_{-1}	$0.89^{+0.03}_{-0.02}$	$108.5^{+5.0}_{-4.6}$	$0.59^{+0.08}_{-0.06}$	-425	-59206
	23	-125^{+13}_{-8}	-43^{+9}_{-11}	233^{+8}_{-10}	47^{+88}_{-72}	3^{+1}_{-1}	$0.90^{+0.02}_{-0.02}$	$109.4^{+3.9}_{-5.0}$	$0.63^{+0.06}_{-0.06}$	-419	-78158
	23	-128^{+14}_{-11}	-42^{+12}_{-8}	235^{+10}_{-10}	42^{+10}_{-7}	3^{+1}_{-1}	$0.89^{+0.03}_{-0.02}$	$108.5^{+5.0}_{-4.7}$	$0.51^{+0.05}_{-0.04}$	-409	-106063
UMaI	103	145^{+25}_{-24}	-199^{+28}_{-30}	264^{+26}_{-19}	–	–	–	–	–	-12791	-719
	103	143^{+26}_{-21}	-203^{+37}_{-23}	267^{+21}_{-26}	292^{+134}_{-150}	102^{+13}_{-17}	$0.48^{+0.21}_{-0.17}$	$118.8^{+4.2}_{-2.3}$	$6.07^{+4.06}_{-3.71}$	-13089	-17091
	102	145^{+18}_{-21}	-200^{+26}_{-34}	265^{+26}_{-18}	184^{+74}_{-38}	102^{+4}_{-5}	$0.29^{+0.13}_{-0.08}$	$118.6^{+2.9}_{-2.8}$	$3.18^{+1.52}_{-0.74}$	-12921	-33461
UMaII	41	-187^{+7}_{-11}	-30^{+18}_{-24}	284^{+20}_{-16}	163^{+127}_{-57}	40^{+5}_{-7}	$0.61^{+0.13}_{-0.10}$	$95.3^{+3.1}_{-4.0}$	$3.46^{+3.53}_{-1.52}$	-1065	-23240
	41	-188^{+8}_{-11}	-35^{+19}_{-20}	286^{+17}_{-12}	119^{+29}_{-17}	40^{+1}_{-2}	$0.50^{+0.07}_{-0.05}$	$96.1^{+3.2}_{-3.4}$	$2.02^{+0.34}_{-0.23}$	-1225	-43016
	41	-187^{+12}_{-8}	-32^{+23}_{-18}	285^{+21}_{-18}	85^{+21}_{-15}	40^{+2}_{-2}	$0.36^{+0.07}_{-0.06}$	$95.7^{+4.1}_{-3.1}$	$1.37^{+0.23}_{-0.21}$	-1137	-67198

©2021 Astronomical and Astrophysical Transactions (AApTr), Vol. 32, Issue 3

Table 4 (continued)

Name	d_{GC} [kpc]	Π [km/s]	Θ [km/s]	V_{tot} [km/s]	apo [kpc]	peri [kpc]	ecc	incl. θ [deg]	T_r [Gyr]	L_Z [kpc km/s]	E [(km/s)^2]
UMiI	78	54^{+4}_{-4}	23^{+6}_{-5}	160^{+4}_{-4}	98^{+8}_{-6}	49^{+4}_{-4}	$0.33^{+0.04}_{-0.03}$	$83.4^{+1.7}_{-1.3}$	$2.24^{+0.21}_{-0.16}$	1316	−29689
	79	50^{+4}_{-4}	21^{+8}_{-5}	159^{+4}_{-3}	90^{+6}_{-4}	44^{+4}_{-4}	$0.34^{+0.04}_{-0.03}$	$83.8^{+2.1}_{-1.5}$	$1.69^{+0.11}_{-0.08}$	1213	−48906
	78	52^{+4}_{-4}	23^{+6}_{-6}	160^{+3}_{-3}	86^{+4}_{-4}	39^{+3}_{-3}	$0.38^{+0.03}_{-0.03}$	$83.5^{+1.8}_{-1.6}$	$1.37^{+0.06}_{-0.07}$	1282	−67144
Wil1	43	-63^{+12}_{-9}	53^{+19}_{-15}	121^{+11}_{-9}	44^{+3}_{-1}	16^{+3}_{-2}	$0.46^{+0.05}_{-0.06}$	$72.7^{+5.5}_{-4.8}$	$0.72^{+0.07}_{-0.03}$	1523	−54328
	43	-65^{+9}_{-13}	48^{+14}_{-21}	120^{+12}_{-7}	44^{+2}_{-2}	17^{+3}_{-2}	$0.43^{+0.04}_{-0.07}$	$74.1^{+3.9}_{-6.8}$	$0.74^{+0.06}_{-0.04}$	1387	−74801
	43	-64^{+8}_{-11}	51^{+20}_{-19}	121^{+13}_{-5}	44^{+2}_{-2}	15^{+3}_{-1}	$0.48^{+0.03}_{-0.06}$	$73.2^{+5.6}_{-6.5}$	$0.64^{+0.05}_{-0.02}$	1473	−98215

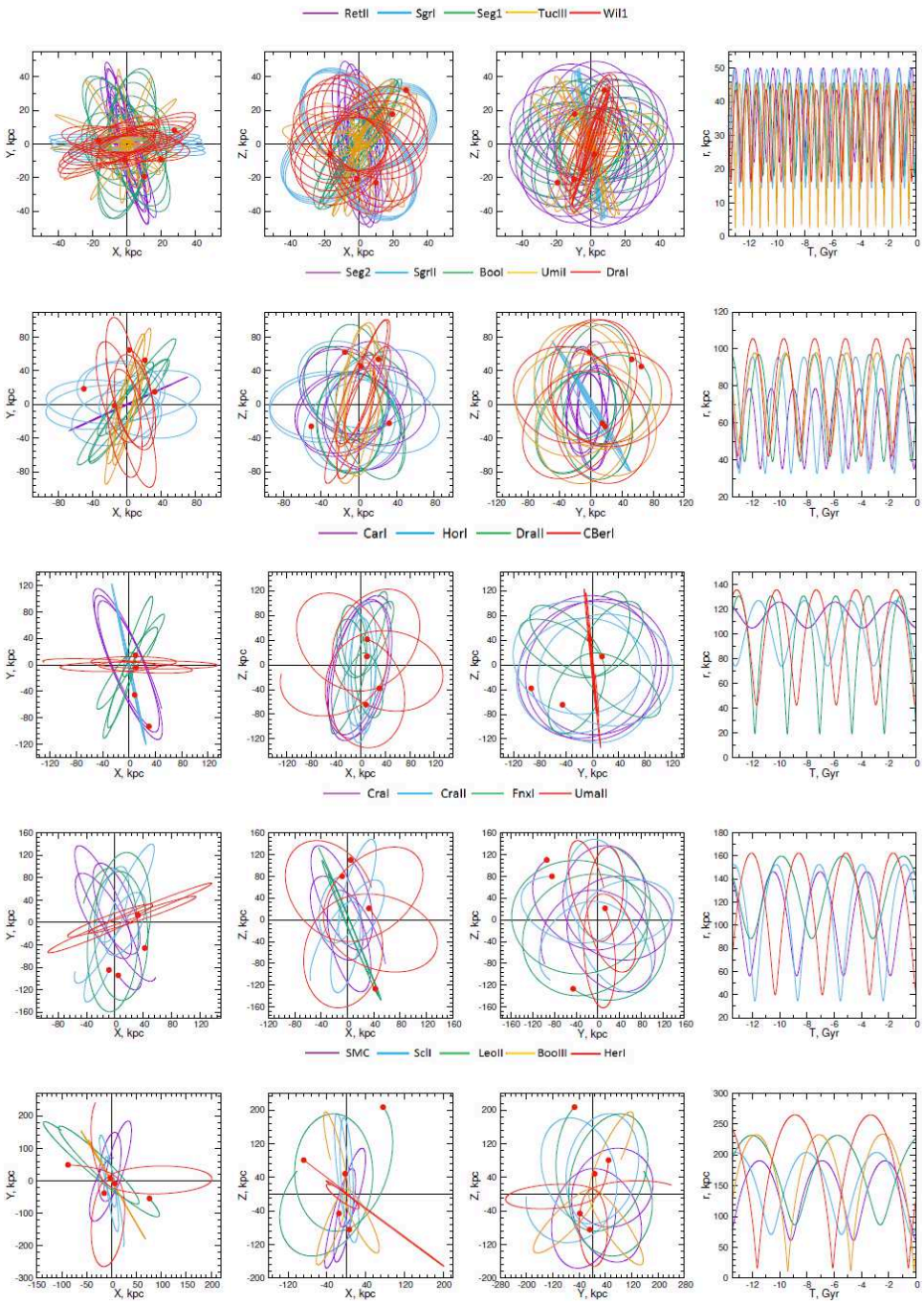


Figure 5 Orbits of the dwarf galaxies in the galactic potential NFWBB.

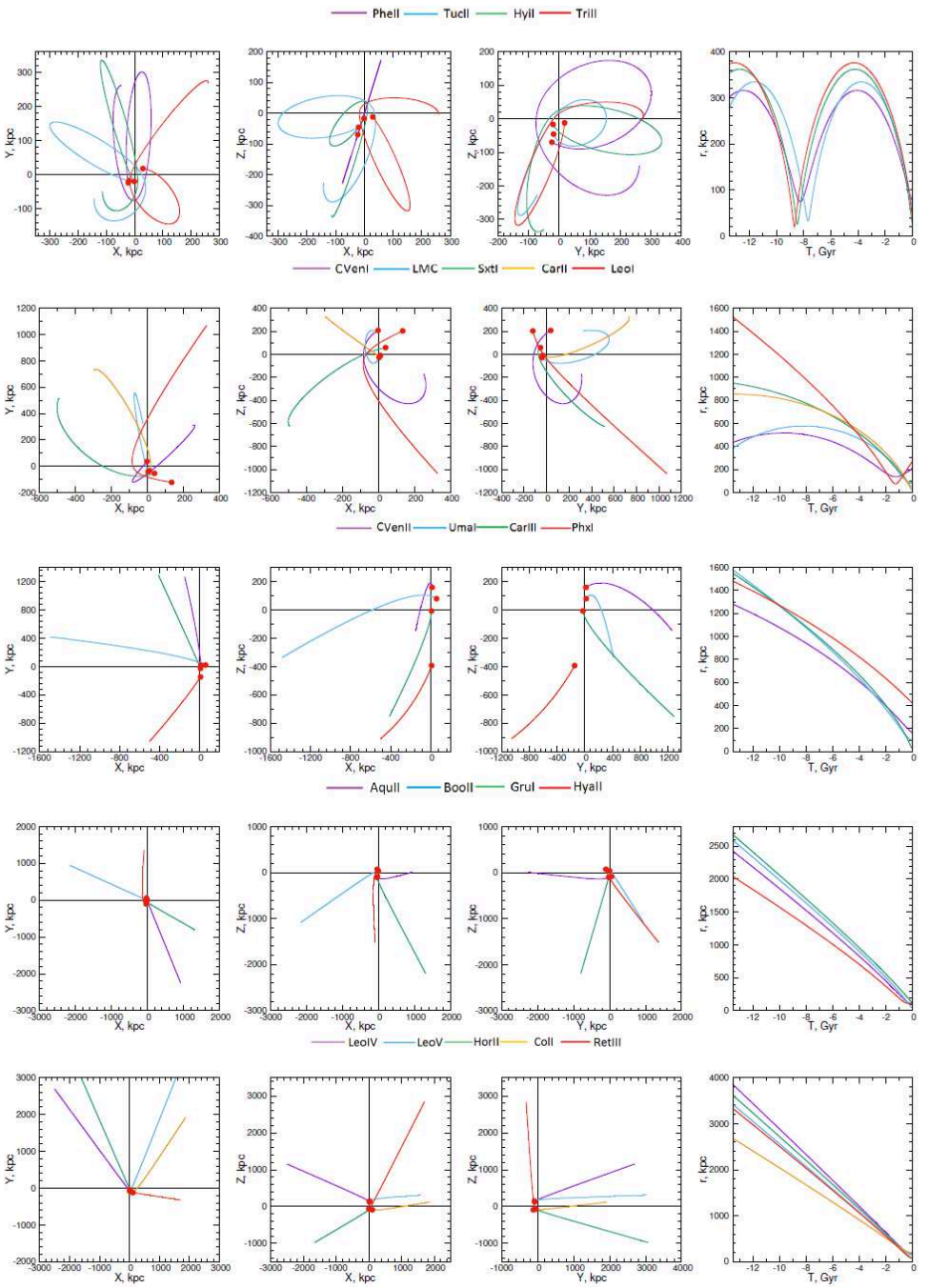


Figure 5 (continued)

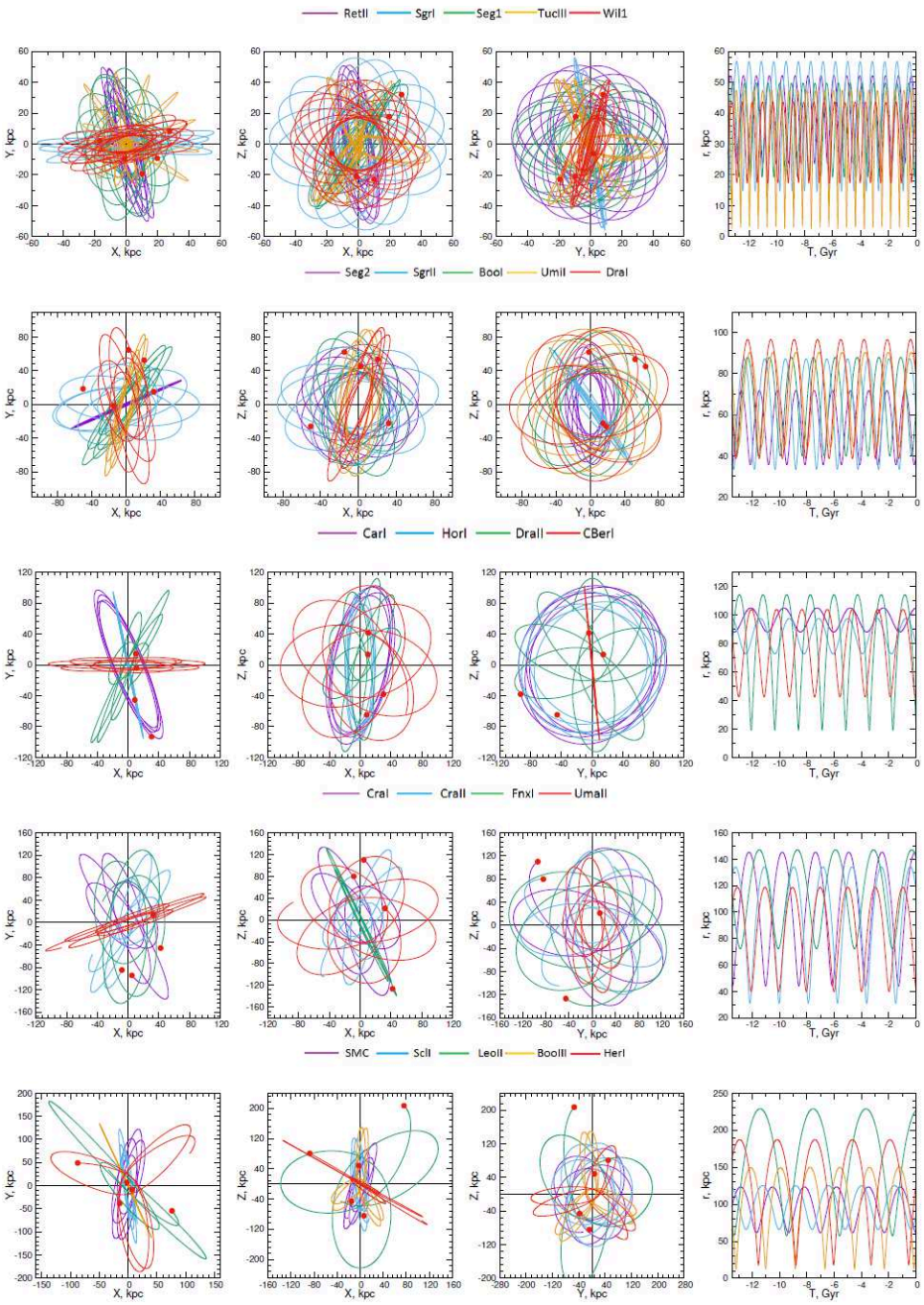


Figure 6 Orbits of the dwarf galaxies in the galactic potential ASBB.

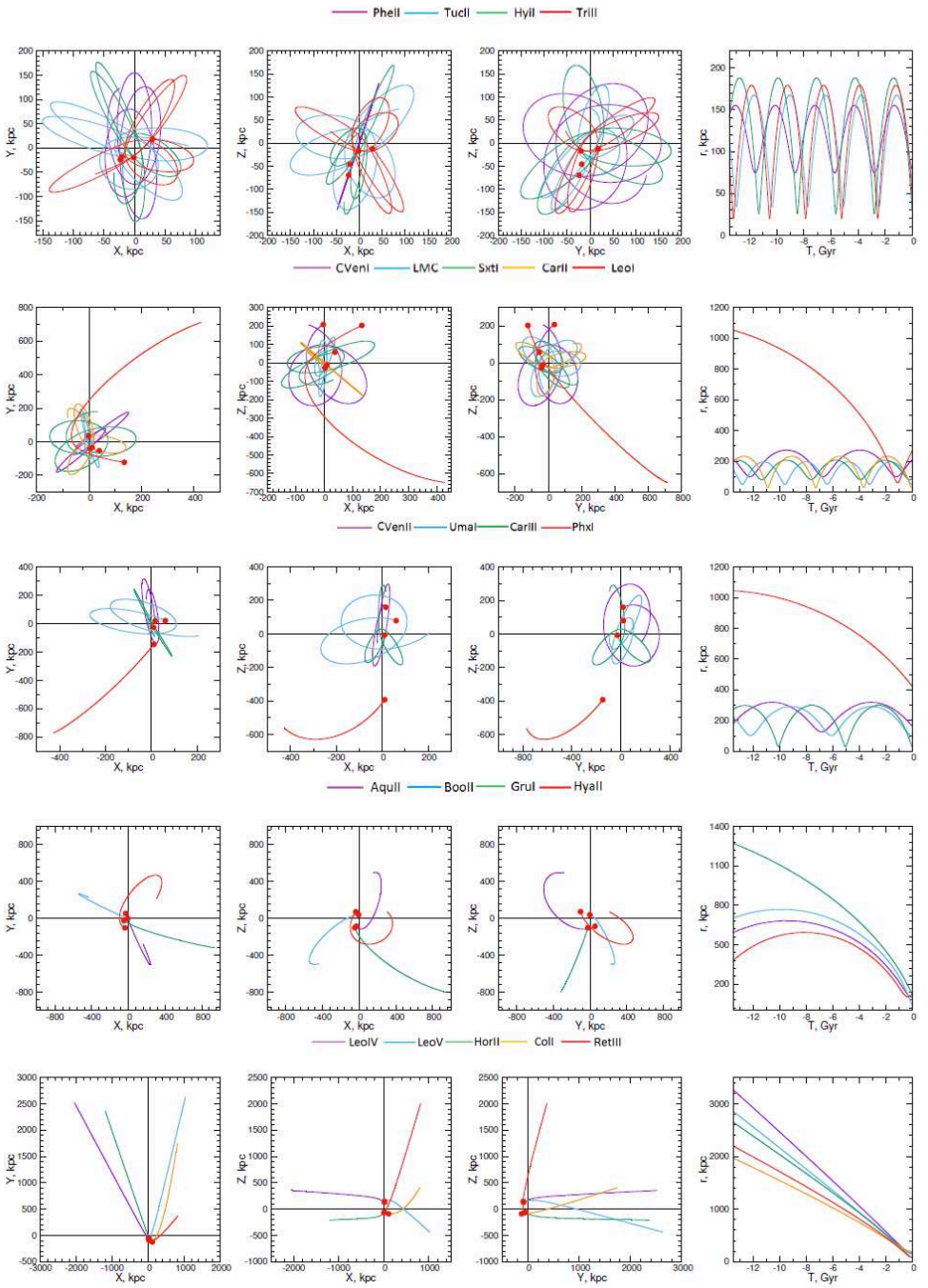


Figure 6 (continued)

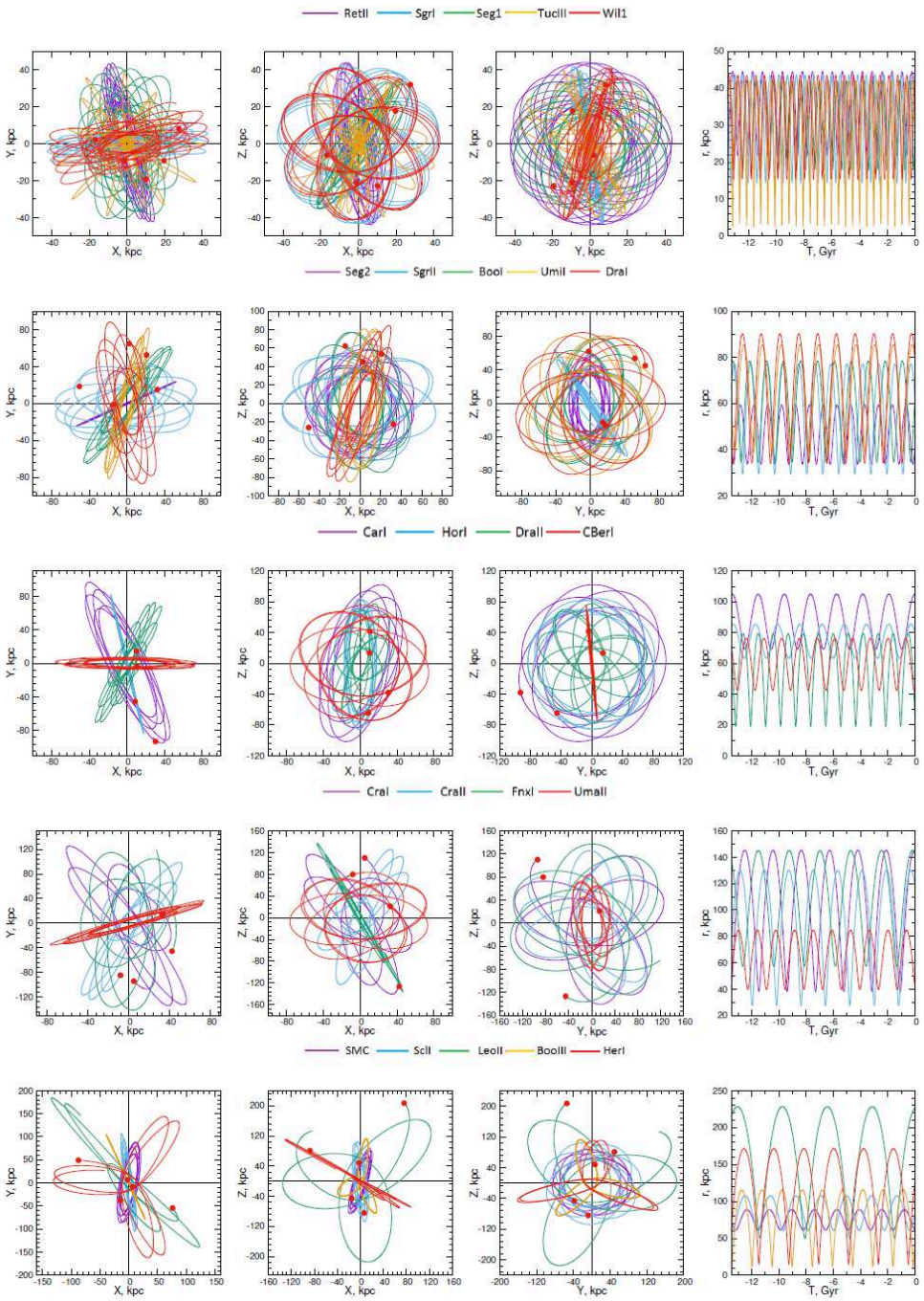


Figure 7 Orbits of the dwarf galaxies in the galactic potential ASI.

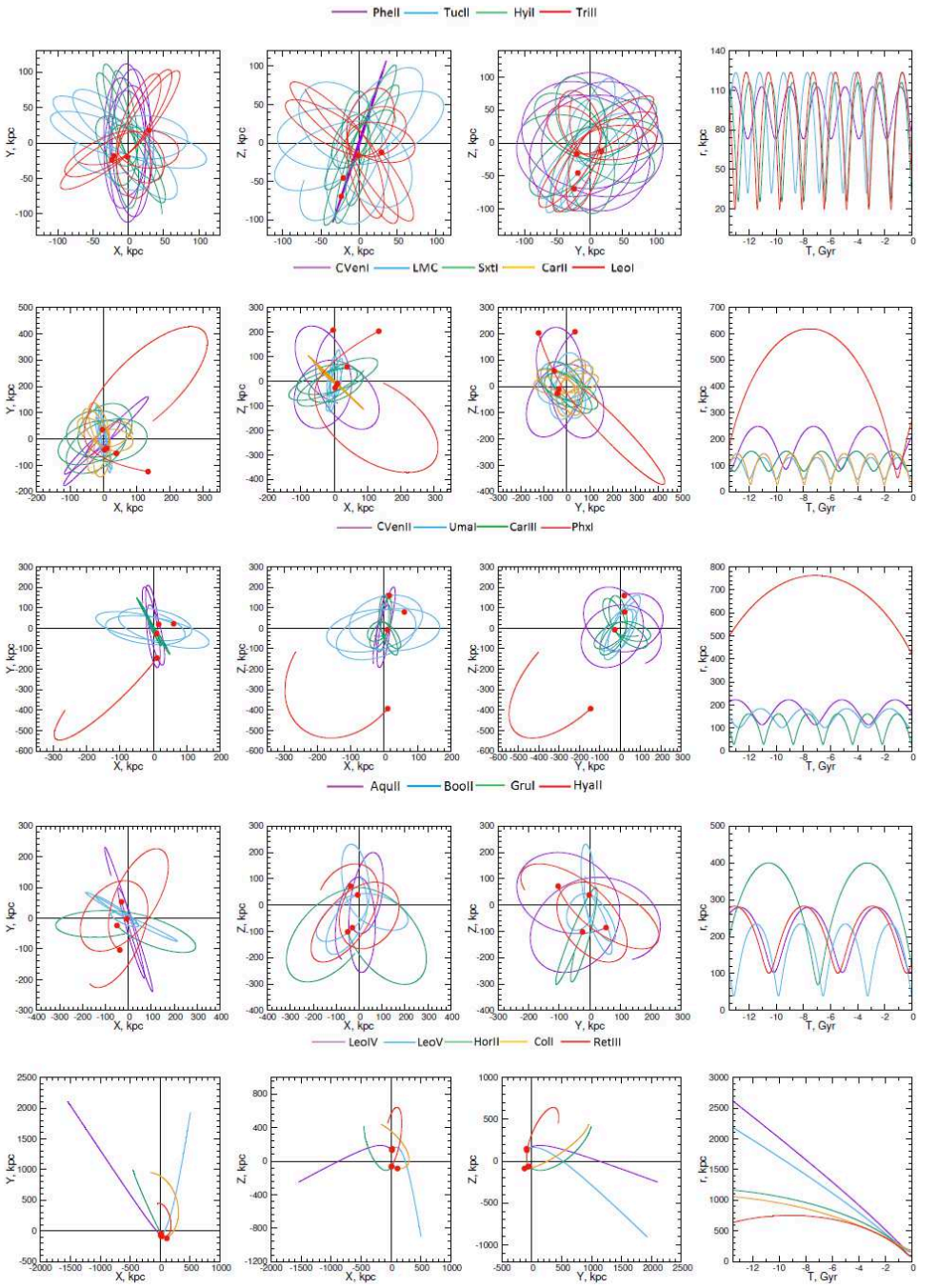


Figure 7 (continued)

We do not give the orbits of two dwarf galaxies EriII and PisII, which in all three potentials do not show the gravitational connection with the Milky Way. In the Figures we give (X,Y), (X,Z), (Y,Z) projections for each orbit in Cartesian galactic coordinate system, as well as a radial coordinate of the orbit r as a function of time T. The latter gives us an idea of the periodicity of the orbit. To save space, each panel represents the orbits of 5-4 objects, the names of which are given above the pictures. Mostly objects are grouped by proximity of scale.

5.1 Gravitational connection of the dwarf galaxies with the Milky Way

One of the main questions in the study of the dynamics of dwarf galaxies is their gravitational connection with the Milky Way. Figure 3 shows the diagrams $L_Z - E$, calculated for three models NFWBB, ASBB and ASI of the galactic potential with different masses $M_{G_{(R\leq 200kpc)}} = 0.75, 1.45$ and 1.9 of $10^{12}M_\odot$, respectively. The area of positive energy values E is shown in gray. The dwarf galaxies that are not gravitationally associated with the Milky Way, having velocities V_{tot} higher than the escape velocities, belong to this area. In the case of the model NFWBB, these are 11 dwarf galaxies (AquII, BooII, ColI, EriII, GruI, HorII, HyaII, LeoIV, LeoV, PisII, RetIII), in the case of the model ASBB, 7 galaxies (ColI, EriII, HorII, LeoIV, LeoV, PisII, RetIII), and in the case of the model ASI, 4 galaxies (EriII, LeoIV, LeoV, PisII). Note that in Table 4 for such dwarfs the orbit parameters apo, peri, ecc, θ and T_r are not determined. There are also several dwarf galaxies with a very weak gravitational connection with the Milky Way (CVenII, CarIII, SxtI, UmaI in NFWBB model, LeoI both in NFWBB and ASBB models, PhxI in all three models). There are several dwarf galaxies with a very weak gravitational connection with the Milky Way. Although they are characterized by negative total energy E, it is not enough for reliable determination of orbital parameters. Table 4 and Figs. 5–7 allow us to trace the dependence of the orbital motion of the dwarf galaxies on the model of the galactic gravitational potential and mass of the Galaxy. Thus, the mass of the Galaxy determines degree of gravitational connection with dwarf galaxies. Therefore, further work on refining the rotation curve of our Galaxy and on this basis refining a model of its potential and mass is of great importance.

5.2 The comparison of the orbits integrated in the three models of the galactic potential

In Fig. 4 we present a comparison of the orbital parameters of the dwarf galaxies obtained using three models (NFWBB, ASBB, ASI) of the galactic potential. These parameters are apo, peri, ecc, Z_{max}, T_r and E. Other orbital parameters listed in Table 4 ($\Pi, \Theta, V_{tot}, \theta, L_Z$) depend slightly on the model of the galactic potential, therefore, we do not give graphs of their comparison.

In Fig. 4 the parameters obtained in the ASBB (black triangles) and the ASI (red dots) models of the galactic potential are compared with corresponding orbit parameters obtained in the NFWBB model. In each panel the line of coincidence is plotted. It can be seen from the pictures that with an increase in the mass of the Galaxy, at large distances, where the rotation curves of the Galaxy corresponding to the different models of the potential diverge significantly, the parameters apo,

peri, Z_{max}, T_r tend to decrease in magnitude. Almost all points in the pictures are below the coincidence line. The behavior of the eccentricity, which depends on both apocentric and pericentric distance, is different for different objects. For majority of the dwarfs the eccentricity decreases with an increase of the mass of the Galaxy. That is, a larger mass of the Galaxy leads to a more circular orbit. The total energy of the dwarfs with an increase in the mass of the Galaxy proportionally shifts to a more negative zone, parallel to the coincidence line, since the fraction of potential energy, which is negative, increases.

It is currently difficult to determine the only valid Galaxy model. This problem requires further refinement of the model of the Galaxy and its mass. Further refinement of the three-dimensional dynamics of galactic objects also requires further refinement of astrometric data.

6 Conclusions

(i) Based on modern literary data on positions, proper motions (from Gaia DR2 Catalog), and line-of-sight velocities, a sample of 47 dwarf satellite galaxies of the Milky Way was formed to analyze their orbital motion using three models of the galactic potential with different masses.

(ii) To select the most probable models of the galactic potential, we collected the Galaxy mass estimates from various literary sources obtained by independent methods. As a result, three models were selected that describe the axisymmetric potential of the Galaxy: 1) the model with a dark halo in the NFW form, modified by Bajkova & Bobylev (2016) (NFWBB), 2) the Allen & Santillán (1991) model, also modified in Bajkova & Bobylev (2016) (ASBB) and 3) the Allen & Santillán (1991) model, modified by Irrgang et al. (2013) (ASI), with low($M_{G_{(R\leq 200kpc)}} = 0.75 \times 10^{12} M_{\odot}$), middle ($M_{G_{(R\leq 200kpc)}} = 1.45 \times 10^{12} M_{\odot}$) and high ($M_{G_{(R\leq 200\ kpc)}} = 1.9 \times 10^{12} M_{\odot}$) mass of the Galaxy, respectively.

(iii) We present the orbits and the orbit properties of the dwarf galaxies obtained by integration for 13.5 Gyr backward in the three models of the galactic potential. We give a comparison of the orbital parameters corresponding to different models of the galactic potential.

(iv) For each model of the galactic potential we have identified dwarf galaxies that are not connected gravitationally with the Milky Way. For the NFWBB model these are AquII, BooII, ColI, EriII, GruI, HorII, HyaII, LeoIV, LeoV, PisII, RetIII, for the ASBB model, ColI, EriII, HorII, LeoIV, LeoV, PisII, RetIII), and for the ASI model, EriII, LeoIV, LeoV, PisI.

At this stage of research, it is difficult to say which model of the Galaxy is the most realistic. Further refinement of the rotation curve of the Galaxy is required, especially at large distances from the center of the Galaxy in order to refine the model of the Galaxy and its mass. Further refinement of the three-dimensional dynamics of galactic objects also requires further refinement of astrometric measurements.

References

Ablimit I., Zhao G., Flynn C.,and Bird S.A. (2020) ApJ 895, L12
Aihara H., Prieto C.A., An D., et al. (2011) ApJ Suppl. 193, 29
Allen C., Martos M. (1986) RMxAA 13, 137
Allen C., Santillán A. (1991) RMxAA 22, 255
Bajkova A.T., Bobylev V.V. (2016) Ast. Lett. 42, 567
Bajkova A.T., Bobylev V.V. (2017a) OAst 26, 72
Bajkova A.T., Bobylev V.V. (2017b) Ast. Rep. 61, 727
Battaglia G., Helmi A., Morrison H., et al. (2005) MNRAS 364, 433
Bhattacharjee P., Chaudhury S., Kundu S., and Majumdar S. (2013) Phys. Rev. D 87, id.083525
Bhattacharjee P., Chaudhury S., and Kundu S. (2014) ApJ 785, 63
Bobylev V.V., Bajkova A.T. (2016) Ast. Lett. 42, 1
Bobylev V.V., Bajkova A.T., and Gromov A.O. (2017) Ast. Lett. 43, 241
Gaia Collaboration, Brown A.G.A., Vallenari A., Prusti T., et al. (2018) A&A, 616, id.A1
Callingham T.M., Cautun M., Deason A.J., et al. (2019) MNRAS 484, 5453
Deason A.J., Belokurov V., Evans N.W., and An J. (2012a) MNRAS 424, L44
Deason A.J., Belokurov V., Evans N.W., et al. (2012b) MNRAS 425, 2840
Deason A.J., Fattahi A., Frenk C.S., et al. (2020) MNRAS 496, 3929
Dehnen W., Binney J. (1998) MNRAS 294, 429
Deng L.-C., Newberg H.J., Liu C., et al. (2012) Res. Astron. Astrophys. 12, 735
Drlica-Wagner A., Bechtol K., Mau S., et al. (2020) ApJ 893, id.47
Eadie G.M., Harris W.E., and Widrow L.M. (2015) ApJ 806, 54
Eadie G.M., Jurić M. (2019) ApJ 875, 159
Fardal M.A., van der Marel R.P., Law D.R., et al. (2019) MNRAS 483, 4724
Fritz T.K., Battaglia G., Pawlowski M.S., et al. (2018) A&A 619, 103
Fritz T.K., Carrera R., Battaglia G., and Taibi S. (2019) A&A 623, 129
Fritz T.K., Di Cintio A., Battaglia G., et al. (2020) MNRAS 806, 54
Gibbons S.L.J., Belokurov V., and Evans N.W. (2014) MNRAS 445, 3788
Gnedin O.Y., Brown W.R., Geller M.J., and Kenyon S.J. (2010) ApJ 720, L108
Gaia Collaboration, Helmi A., van Leeuwen F., McMillan P.J., et al. (2018) A&A 616, 12
Helmi A. (2020) Ann. Rev. Astron. Astrophys. 58, 205
Hernitschek N., Sesar B., Rix H.-W., et al. (2017) ApJ 850, 96
The HIPPARCOS and Tycho Catalogues. (1997) ESA SP–1200
Huang Y., Liu X.-W., Yuan H.-B., et al. (2016) MNRAS 463, 2623
Irrgang A., Wilcox B., Tucker E., and Schiefelbein L. (2013) A&A 549, 137
Kafle R.R., Sharma S., Lewis G.F., and Bland-Hawthorn J. (2012) ApJ 761, 98
Kallivayalil N., van der Marel R.P., Besla G., et al. (2013) ApJ 764, 161
Gaia Collaboration, Kallivayalil N., Sales L.V., Zivick P., et al. (2018) ApJ 867, 19
Karachentsev I.D., Kashibadze O.G., Makarov D.I., and R.B. Tully. (2009) MNRAS 393, 1265
Gaia Collaboration, Lindegren L., Hernandez J., Bombrun A., et al. (2018) A&A 616, 2
Longeard N., Martin N., Starkenburg E., et al. (2020) MNRAS 491, 356

Van der Marel R.P. (2015) Proc. IAU Symp. 311, 1
Massari D., Helmi A. (2018) A&A, 620, 155
Massari D., Koppelman H.H., and Helmi A. (2019) A&A 630, id.L4
McConnachie A.W. (2012) AJ 144, 4
McMillan P.J. (2011) MNRAS 414, 2446
Miyamoto M., Nagai R. (1975) PASJ 27, 533
Nadler E.O., Wechsler R.H., Bechtol K., et al. (2020) ApJ 893, id.48
Navarro J.F., Frenk C.S., and White S.D.M. (1997) ApJ 490, 493
Newton O., Cautun M., Jenkins A., et al. (2018) MNRAS 479, 2853
Pace A.B., Li T.S. (2019) ApJ 875, 77
Pace A.B., Kaplinghat M., Kirby E., et al. (2020) MNRAS 495, 3022
Patel E., Besla G., Mandel K., and Sohn S.T. (2018) ApJ 857, 78
Pato M., Iocco F. (2015) ApJ 803, L3
Pawlowski M.S., Kroupa P. (2013a) MNRAS 435, 1928
Pawlowski M.S., Kroupa P. (2013b) MNRAS, 435, 2116
Pojmanski G. (2002) Acta Astron. 52, 397
Posti L., Helmi A. (2019) A&A 621, 56
Gaia Collaboration, Prusti T., de Bruijne J.H.J., Brown A.G.A., et al. (2016) A&A 595, id.A1
Pryor C., Piatek S., and Olszewski E.W. (2010) AJ 139, 839
Pryor C., Piatek S., and Olszewski E.W. (2015) AJ 149, 42
Schönrich R., Binney J., and Dehnen W. (2010) MNRAS 403, 1829
Simon J. (2018) ApJ 863, 89
Sofue Y. (2012) PASJ 64, 75
Sofue Y. (2017) PASJ 69, 1
Udalski A., Kubiak M., and Szymański M. (1997) Acta Astron. 47, 319
Wang W., Han J., Cautun M., et al. (2020) SCPMA, 63, id.109801
Watkins L.L., Evans N.W., and An J.H. (2010) MNRAS 406, 264
Xue X.X., Rix H.W., Zhao G., et al. (2008) ApJ 684, 1143
Yanny B., Rockosi C., Newberg H.J., et al. (2009) AJ 137, 4377